# Plant Physiology®

https://doi.org/10.1093/plphys/kiaf033 Advance access publication 28 January 2025

Research Article

# Inhibition of mitochondrial energy production leads to reorganization of the plant endomembrane system

Taotao Wang, Xinjing Li, Hongying Yu, Heng Zhang, D Zhiping Xie, D Qingqiu Gong

State Key Laboratory of Microbial Metabolism & Joint International Research Laboratory of Metabolic and Developmental Sciences, School of Life Sciences and Biotechnology, Shanghai Jiao Tong University, Shanghai 200240, P. R. China

\*Author for correspondence: gongqingqiu@sjtu.edu.cn (Q.G.)

The author responsible for distribution of materials integral to the findings presented in this article in accordance with the policy described in the Instructions for Authors (https://academic.oup.com/plphys/pages/General-Instructions) is: Qingqiu Gong (gongqingqiu@sjtu.edu.cn).

#### **Abstract**

Mitochondria have generated the bulk of ATP to fuel cellular activities, including membrane trafficking, since the beginning of eukaryogenesis. How inhibition of mitochondrial energy production will affect the form and function of the endomembrane system and whether such changes are specific in today's cells remain unclear. Here, we treated Arabidopsis thaliana with antimycin A (AA), a potent inhibitor of the mitochondrial electron transport chain (mETC), as well as other mETC inhibitors and an uncoupler. We investigated the effects of AA on different endomembrane organelles connected by vesicle trafficking via anterograde and retrograde routes that heavily rely on ATP and GTP provision for SNARE and RAB/GEF function, respectively, in root cells. Similar to previous reports, AA inhibited root growth mainly by shortening the elongation zone (EZ) in an energy- and auxin-dependent way. We found that PIN-FORMED 2 (PIN2) and REQUIRES HIGH BORON 1 (BOR1), key proteins for EZ establishment and cell expansion, undergo accelerated endocytosis and accumulate at enlarged multivesicular bodies (MVBs) after AA treatment. Such accumulation is consistent with the observation that the central vacuole becomes fragmented and spherical and that the Arabidopsis Rab7 homolog RABG3f, a master regulator of MVB and vacuolar function, localizes to the tonoplast, likely in a GTP-bound form. We further examined organelles and vesicle populations along the secretory pathway and found that the Golgi apparatus—in particular, the endoplasmic reticulum—Golgi intermediate compartment (ERGIC)—cannot be maintained when mETC is inhibited. Our findings reveal the importance and specific impact of mitochondrial energy production on endomembrane homeostasis.

# Introduction

Mitochondria are powerhouses of eukaryotic cells and had been essential in the evolution of eukaryotes (Roger et al. 2017; Møller et al. 2021; Suomalainen and Nunnari 2024). According to eukaryogenesis theories, a bacterial species in the phyllum alphaproteobacteria, was engulfed by an Archaea most closely related to the Asgard superphylum, and this endosymbiotic event probably led to the emergence of last common ancestor of eukaryotes (LECA) (Spang et al. 2015). A great expansion in cellular activities and complexities that accompanied the emergence of LECA has been attributed to the powerful energy production ability of mitochondria (Martin and Müller 1998), for the amount of ATP generated through mitochondrial oxidative phosphorylation (OXPHOS) is at least 14 to 15 folds more than those generated through anaerobic glycolysis.

Mitochondrial energy production is carried out at the cisternae of mitochondrial inner membrane (Millar et al. 2011; Pfanner et al. 2019). Four multiprotein complexes, namely ubiquinone oxidoreductase (Complex I), succinate dehydrogenase (Complex II), ubiquinol-cytochrome c oxidoreductase (Complex III), cytochrome c oxidase (Complex IV), along with soluble electron carriers ubiquinone and cytochrome c, form the mitochondrial electron transport chain (mETC) (Schertl and Braun 2014; Zheng et al. 2024). They establish an electrochemical proton gradient across the inner membrane, which drives ATP production via a proton-driven rotation of ATP synthase (Complex V). Mutations in mETC components are either lethal or are a common cause

of inherited metabolic disorders and inherited neurological disorders in humans (Nunnari and Suomalainen 2012; Gorman et al. 2016); plant mETC mutants are embryonic lethal except for those of Complex I, whose function can be bypassed by rotenone-insensitive, alternative NAD(P)H dehydrogenases (Rasmusson et al. 1999; Møller et al. 2021). mETC inhibitors and uncouplers either inhibits electron transport or terminal ATP production, or dissipate the proton gradient to prevent energy production. They have been powerful tools in dissecting mETC and in studying consequences of energy depletion and mitochondrial reactive oxygen species (ROS) production (Schwarzländer et al. 2009). In fact, George Palade first demonstrated that membrane trafficking consumes energy in 1968 by combining pulse chase labelling and inhibitors of mETC, including cyanide, antimycin A, and oligomycin (Jamieson and Palade 1968).

Inhibition of mitochondrial energy production cause pleiotropic effects in eukaryotes, especially plants. Apart from replication, transcription, and translation, much cellular energy is spent on maintaining cellular structures and their functions. More than one third of cellular ATP is consumed by the plasma membrane (PM) and tonoplast proton ATPases, which maintain a steep pH gradient of up to 2 units, i.e. pH 5 to 6 in the apoplast/vacuole vs. pH 7 in the cytoplasm, and drive secondary active transporters and cell expansion (Neuhaus and Trentmann 2014; Hedrich et al. 2015; Falhof et al. 2016; Martinoia 2018; Li et al. 2022). Furthermore, plant cells consume both ATP and GTP to fuel the assembly and disassembly of

cytoskeletons, which not only determine directional growth of the cell (Gutierrez et al. 2009), but also help maintain the morphology of membrane-bound organelles and serve as highways for vesicle trafficking (Szymanski and Staiger 2018). The most prominent structural complexity of eukaryotic cells is exhibited by the membrane-bound organelles, particularly the endomembrane system (Zeng et al. 2023; Zhuang et al. 2024). The highly dynamic endomembrane system spans from the nuclear envelope to the PM and controls transport within a eukaryotic cell. It is mainly composed of the endoplasmic reticulum (ER), the Golgi apparatus, the endosomal compartments, i.e. trans-Golgi network or early endosome (TGN/EE) and multivesicular bodies/prevacuolar compartments/ late endosome (MVB/PVC/LE), the vacuole/lysosomes, and the PM. Vesicles carrying macromolecules constantly traverse between the organelles, resembling vehicles on highways that deliver passengers and cargoes (Aniento et al. 2022). Generally, vesicles form and bud from a donor membrane, shuttle along the cytoskeleton, and arrive at and fuse with a target membrane, leading to the delivery of cargo from the donor to the target organelle. Each step is regulated by specific proteins and complexes, including adaptor and coat protein complexes, GTPases, soluble N-ethylmaleimide-sensitive factor attachment protein receptors (SNAREs) and the AAA-ATPase N-ethylmaleimide-Sensitive Factors (NSFs), and tethering complexes (Minamino and Ueda 2019; González Solís et al. 2022). Many of these proteins and complexes are fueled by ATP or GTP hydrolysis, thus consumes cellular energy. However, how mitochondrial energy production specifically affects the form and function of the endomembrane system rather than inhibiting synthesis of proteins functioning in membrane trafficking is still largely unknown.

In this study, we provide a bird's eye view of how antimycin A (AA), as well as other mETC inhibitors and uncoupler, affect the form and function of the endomembrane system in Arabidopsis thaliana. We examined root cells only to preclude the impact of chloroplasts, and documented the shared and unique effects of mETC inhibitors and uncoupler on individual organelles and vesicles along the endocytic pathway and the secretory pathway, to pinpoint energy deficiency-induced changes in organelle shape and function. Like previously reported (Ivanova et al. 2014; Kerchev et al. 2014; Tivendale and Millar 2022), AA inhibited root development in an ATP- and auxin-dependent way, and a major consequence of AA treatment is the inhibition of cell expansion. We further dissected how membrane trafficking of key proteins that mediate cell expansion and root elongation, such as PIN-FORMED 2 (PIN2) and REQUIRES HIGH BORON 1 (BOR1), are specifically affected, and found that both are subject to enhanced endocytosis for vacuolar degradation, with some trapped at enlarged MVBs/LEs. Strikingly, protein trafficking appeared to be depleted from both sides of the TGN/EEs. On one side, MVBs/LEs are enlarged, but vacuoles became fragmented and spherical, with RABG3f stuck on the tonoplast likely in a GTP-bound, activated form. On the other side, Golgi number and shape could no longer be maintained, and the endoplasmic reticulum-Golgi intermediate compartment (ERGIC) disappeared. Our study provides a cell biology view of how endomembrane trafficking and organelles are affected by inhibiting mitochondrial energy production.

# Results

# Antimycin A depolarizes mitochondria and inhibits cell expansion

To evaluate how reduced mitochondrial energy production would affect the cell and its organelles, we examined Arabidopsis seedling roots in all experiments, like previous reports (Ivanova et al. 2014; Kerchev et al. 2014), trying to reduce the involvement of chloroplasts. Notably, the interaction between mitochondria and chloroplasts cannot be eliminated since plastids in the roots (i.e. heterotrophic plastids) are also affected by ATP depletion. For example, the import of ATP from the cytosol into the plastids facilitates starch biosynthesis in heterotrophic plastids (Tjaden et al. 1998; Smith 2008). We first quantified the inhibitory effects of antimycin A (AA) on root growth. One micromolar AA significantly inhibited additional primary root elongation of 5-d-old seedlings over the next 7 d, and at 50 µM, no additional elongation was observed by Day 12 (Fig. 1, A and B). To see whether the growth inhibition is indeed caused by energy reduction, we measured cytosolic ATP levels in the root tip with AT1.03, a geneticallyencoded fluorescence resonance energy transfer (FRET)-based ATP biosensor (Imamura et al. 2009). (Figure 1, C and D). AT1.03 was based on the bacterial  $\epsilon$  subunit, which binds but does not hydrolyze ATP. ATP-induced conformational change in AT1.03 brings the N-terminal mseCFP to the vicinity of the C-terminal cp173-mVENUS to increase FRET efficiency; hence ATP levels can be measured by the Venus/CFP fluorescence emission ratios (Imamura et al. 2009). We found that ATP levels in root tip cells were greatly reduced by AA, and further examined the effects of other classic mETC inhibitors and uncoupler. Rotenone and oligomycin are classic Complex I and Complex V (the F1F0-ATPase) inhibitors, and FCCP (carbonyl cyanide p-trifluoromethoxyphenyl hydrazone) is a potent uncoupler. Like AA, oligomycin and FCCP greatly reduced ATP levels (Fig. 1, C and D). In contrast, rotenone treatment led to higher ATP levels (Fig. 1, C and D), which is expected, since mETC of plants and fungi can bypass Complex I via non-proton pumping NAD(P)H oxidases especially under stress conditions (Garmier et al. 2008).

We then confirmed the AA-induced impairment of mitochondrial function by staining with tetramethylrhodamine ethyl ester (TMRE), a positively charged fluorescent dye sensitive to membrane potential (Supplementary Fig. S1, A and B; Fig. 1, C and D) (Ma et al. 2021). Under normal growth conditions, TMRE stained nearly all mitochondria in root epidermal cells. Depolarized mitochondria without TMRE staining can be observed upon 1 µM AA treatment (Supplementary Fig. S1, A and B), and 10 to 50  $\mu$ M AA completely prevented TMRE staining (Supplementary Fig. S1, A and B; Fig. 1, E and F). Upon 10 µM AA treatment, mitochondrial protein levels were unaffected (Supplementary Fig. S1C). However, most mitochondria failed to maintain cristae and became vacuolated (Fig. 1, G and H; Supplementary Fig. S1, E and F). Upon 20 μM AA treatment, root epidermal cells started to lose PM integrity, as Propidium Iodide (PI)-staining of nuclei was observed in Fluorescein Diacetate (FDA)-PI staining of roots (Supplementary Fig. S1D). These imaging results confirmed the detrimental effects of AA on mitochondrial structure and function. Based on these observations, we used 1 to 20 µM AA in most of the following experiments.

The inhibitory effect of AA on primary root elongation indicated hormonal changes like the interaction of auxin and cytokinin in regulating the root apical meristem (RAM) and the elongation zone (EZ) (Schaller et al. 2015). We hence examined the sizes of the RAM, which reflects meristematic cell division, and the EZ, which reflects cell expansion rate. Both RAM and EZ were reduced in length in AA-treated seedlings (Fig. 2, A to D). Reduced transcript levels of key genes in cell expansion, such as the cell wall expansins EXPA1, 4, 6, 8, and 9, and endoglucanases CEL1 and KOR1, were observed (Fig. 2E). The shortened EZ and the reduced expression of key genes in cell expansion suggested that auxin level at the root tip may be reduced. The fluorescent

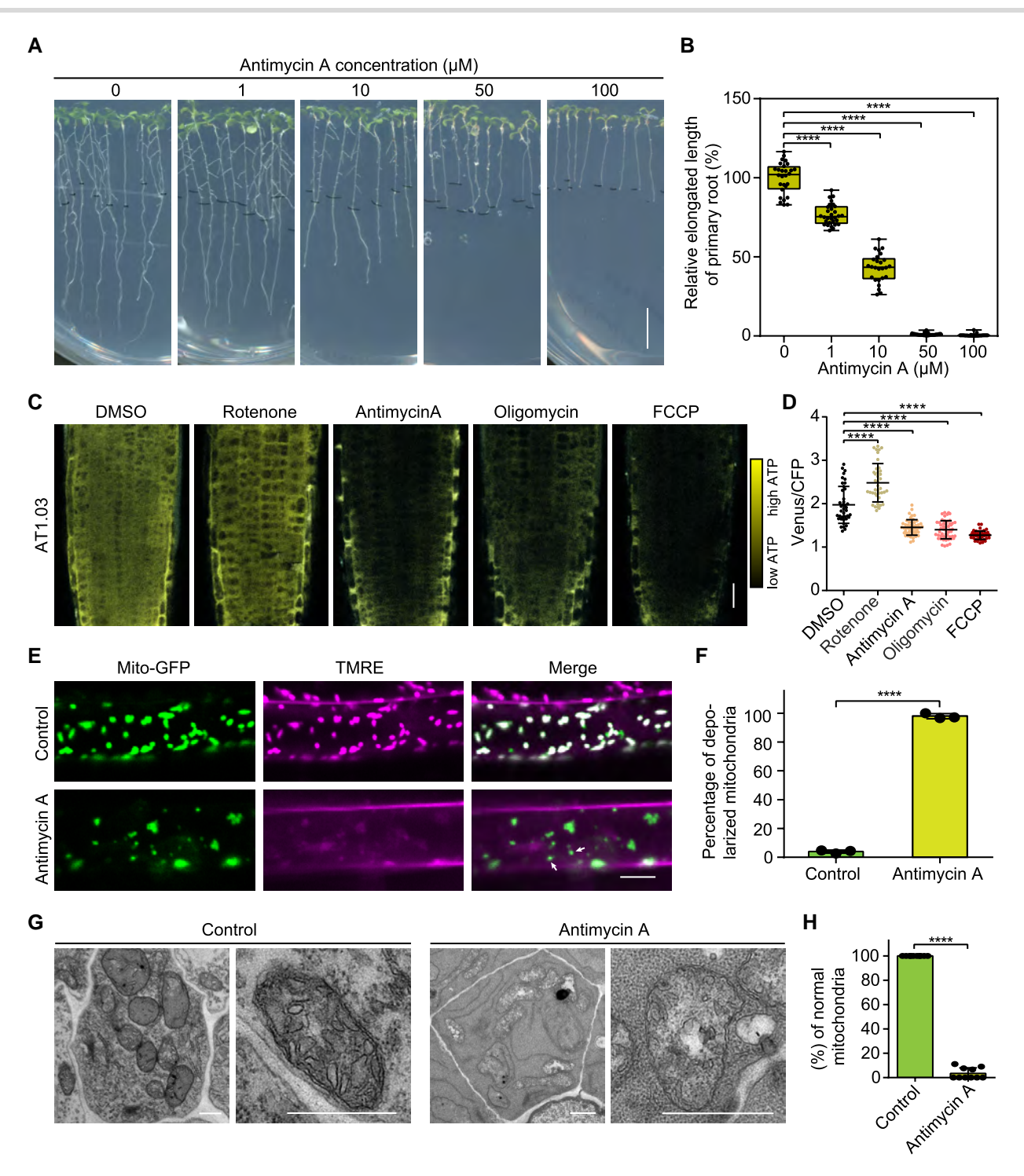


Figure 1. Antimycin A inhibits primary root elongation and impairs structure and function of mitochondria. A) Phenotype of Arabidopsis (Columbia-0) grown on 1/2 Murashige and Skoog (MS) medium supplemented with different concentrations (0, 1, 10, 50, and 100 µM) of antimycin A (AA). Five-day-old vertically grown seedlings were transferred to 1/2 MS medium containing AA and grown vertically for another 7 d. Bar = 1 cm. B) Quantification of relative primary root elongation on AA in (A). Additional primary root elongation on ½ MS was set as 100%. Center lines, box range, whiskers, and points indicate the median, lower to upper quartile, 1.5 x interquartile, and statistical duplication, respectively. Data are mean values ± SD from >15 seedlings of 3 biological replicates. \*\*\*\*, P < 0.0001, Student's t-test. C) Cytosolic ATP levels in root tip cells, indicated by the AT1.03 ATP biosensor, are greatly reduced by AA, oligomycin, and FCCP, but not by rotenone. Five-d-old seedlings were treated with 20  $\mu$ M drugs for 2 h before imaging. Bar = 20  $\mu$ m. D) Quantification of FRET signals (Venus/CFP fluorescence emission ratios) in C), reflecting ATP levels in living cells. Data are mean values ± SD from > 15 roots from three biological replicates. \*\*\*\*, P < 0.0001, Student's t-test. **E)** Mitochondrial membrane depolarization induced by AA. Confocal micrographs of 5-d-old WT root cells expressing a mitochondrion-targeted GFP (mito-GFP) after incubation with dimethyl sulfoxide (DMSO) or 10 µM AA for 2 h. Mitochondria were pre-stained with 100 nm TMRE (tetramethylrhodamine, ethyl ester) for 30 min before imaging. Arrows indicated the depolarized mitochondria after AA treatment. Bar =  $5 \mu m$ . F) Quantification of percentages of depolarized mitochondria in E). Data are mean values  $\pm$  SD from about 500 mitochondria from five samples per condition. \*\*\*\*, P < 0.0001, Student's t-test. G) Transmission Electron Microscopy (TEM) of mitochondria in WT root tip cells incubated with DMSO or 10 µM AA for 2 h. Bar = 500 nm. H) Quantification of percentage of normal-looking mitochondria in G). Nearly all mitochondria lost crista and became vacuolated upon AA treatment. Data are mean values ± SD of > 10 cells from three biological replicates. \*\*\*\*, P < 0.0001, Student's t-test.

intensity of DR5rev:GFP, a marker for auxin response, was significantly reduced in the columella (Fig. 2, F and G). Supplying AA-treated seedlings with ATP partially rescued the defects in lateral root formation (Supplementary Fig. S2, A and B). The partial rescue phenotype suggested that ROS generated by AA-damaged mitochondria may also affect the sizes of RAM and EZ. Consistent with the partially restored lateral root phenotypes, transcript levels of key genes in cell expansion were restored or partially restored by exogenous ATP (Supplementary Fig. S2C).

# AA accelerates PIN2 and BOR1 endocytosis and vacuolar degradation to reduce their levels at the PM

The auxin efflux carrier PIN2 localizes to the apical PM of lateral root cap (LRC) and epidermal cells in the transition zone to facilitate EZ establishment (Abas et al. 2006; Jásik et al. 2016). PIN2 is highly dynamic as it undergoes endocytosis, exocytosis, recycling back to the PM, and vacuolar degradation. The short EZ phenotype in AA-treated seedlings suggested that PIN2 sub-cellular distribution and membrane trafficking may be interrupted. First we observed that PIN2-GFP fluorescence at the PM was clearly reduced by AA (Supplementary Fig. S2, D and E), whereas PIN2 mRNA level stayed unchanged (Supplementary Fig. S2F). Such reduction thus prompted us to examine PIN2 endocytosis and vacuolar degradation. Starting from 1 µM, AA treatment led to PIN2 accumulation within puncta in the cytoplasm (Fig. 2, H and I). The number of PIN2 puncta increased to reach a peak at 20 µM AA. Timewise, PIN2 puncta can been seen within one hour of AA treatment (Fig. 2, J and K).

We then examined whether other mETC inhibitors and uncoupler can induce PIN2 internalization. Similar to AA, oligomycin induced cytoplasmic PIN2 puncta formation, whereas rotenone had very little effects (Fig. 3, A and B). FCCP strongly reduced PIN2-GFP levels. These observations are consistent with ATP levels observed (Fig. 1C). We then checked the identity of PIN2 puncta. Co-localization of PIN2-GFP and the endocytic tracer FM4-64 was seen in AA-treated cells 2 h after FM4-64 staining (Fig. 3, C and D), a time point when FM4-64 stains mainly MVB/ LE. Partial co-localization was seen between PIN2-GFP and VHA-a1-RFP, the TGN/EE-localized catalytic subunit of the V-ATPase (Dettmer et al. 2006) (Fig. 3, E and F). Furthermore, treating the seedlings concurrently with AA and ES9-17, an endocytosis inhibitor that targets clathrin heavy chain (CHC) in plants (Dejonghe et al. 2019), inhibited cytoplasmic PIN2 puncta formation (Fig. 3, G and H). These observations indicated that, upon AA treatment, PIN2 undergoes accelerated endocytosis and likely accumulated at the MVB/LE.

We then examined whether AA treatment can lead to PIN2-GFP vacuolar degradation. Dark treatment was used to induce vacuolar transport and degradation of PIN2 (Laxmi et al. 2008). First, dark-induced PIN2-GFP vacuolar accumulation was indeed much stronger in AA-treated seedlings (Fig. 3, I and J). Then we blocked protein synthesis with cycloheximide (CHX) to trace PIN2-GFP upon AA and oligomycin treatments. Both AA and oligomycin reduced PIN2 levels at the PM, and quantification of PIN2 protein level in the membrane fraction with western blotting confirmed such reduction (Fig. 3, K to M). Collectively, AA treatment accelerated PIN2 endocytosis toward the vacuole for degradation.

To see whether AA may promote vacuolar degradation of other polar PM proteins to inhibit root growth, we also examined the sub-cellular distribution and trafficking of AUX1, the auxin influx carrier required for primary root elongation and lateral root

formation (Marchant et al. 1999; Yang et al. 2006), and BOR1, the boron exporter required for efficient xylem loading of boron. Particularly, the micronutrient boron is a constituent of primary cell walls and influences the mechanical properties of pectins (Vera-Maldonado et al. 2024), and BOR1 PM localization is tightly regulated. For instance, in excess boron supply, BOR1 undergoes endocytosis and vacuolar degradation, likely to avoid boron toxicity (Takano et al. 2002, 2010). We reasoned that, since AA treatment can reduce primary root elongation and cell expansion, it may also induce AUX1 and BOR1 endocytosis. Indeed, AA-induced internalization of AUX1 and BOR1 (Supplementary Fig. S2, G and H), and the effects of AA on BOR1 endocytosis was also time- and concentration-dependent (Supplementary Fig. S2, I to L). The effects of mETC inhibitors and uncoupler on BOR1 was also comparable to the observations on PIN2, with rotenone having little effect and FCCP the strongest (Supplementary Fig. S3, A and B). Co-localization between BOR1 and the TGN/EE, represented by VHA-a1-RFP, was only seen after AA treatment (Supplementary Fig. S3, C to E), validating AA-induced BOR1 endocytosis. The endocytosis inhibitor ES9-17 also inhibited AA-induced BOR1 endocytosis, largely reducing BOR1 puncta numbers in the cytoplasm (Supplementary Fig. S3, F and G). We also analyzed the protein levels of BOR1 after AA or oligomycin treatment, and saw clear reduction in both (Supplementary Fig. S3, H to J). Therefore, AA affects the sub-cellular distribution of BOR1 and PIN2 similarly, promoting their endocytosis and vacuolar degradation.

# AA reduced TGN/EE protein levels but did not affect their localization

We asked how AA treatment may affect the organelles along the endocytic pathway, including TGN/EE, MVB/LE, and the vacuole. AA reduced protein levels of SYP43, a Qa-SNARE that localize to the TGN (Uemura et al. 2012), and VHA-a1, however the sizes of SYP43 or VHA-a1 puncta were not affected by AA (Supplementary Fig. S4, A to D). Therefore, the amount of proteins at the TGN/EE is reduced, but TGN/EE size and distribution appear to be unaffected by AA.

# AA induces enlargement of MVB/LE

We then evaluated whether MVB/LE is affected by AA treatment. Treating a double transgenic line carrying both a TGN marker VHA-a1-RFP and a MVB marker YFP-ARA7 with AA confirmed that only MVB size and signal intensity increased (Supplementary Fig. S4E). Since MVB functions are regulated by the signaling lipid phosphatidylinositol 3-phosphate (PI3P), we examined how AA can affect mNeonGreen-2xFYVE, a probe that specifically binds PI3P. 2xFYVE puncta enlarged significantly after AA treatment, indicative of enlarged/fused MVB (Fig. 4, A and B). ARA7 and RHA1, two MVB-localized Rab5 homologs, VAMP727, a v-SNARE that mediates fusion events at MVB and tonoplast, and VSR4 and BP-80, two vacuolar sorting receptors, all accumulated on enlarged structures (Fig. 4, C to L; Supplementary Fig. S4F). In a double transgenic line carrying YFP-ARA7 and BP80-mCherry, the signal intensities of the two MVB-localized proteins increased after AA treatment (Fig. 4, M and N).

We also compared the effects of mETC inhibitors and uncoupler on mNeonGreen-2xFYVE, BP-80 and VAMP727. Rotenone did not affect the PI3P probe or MVB-localized proteins, whereas AA and oligomycin had similar effects, and FCCP strongly reduced levels of mNeonGreen-2xFYVE, BP80-mCherry, and mRFP-VAMP727 (Fig. 4, O and P; Supplementary Fig. S4, G to J). Observation on

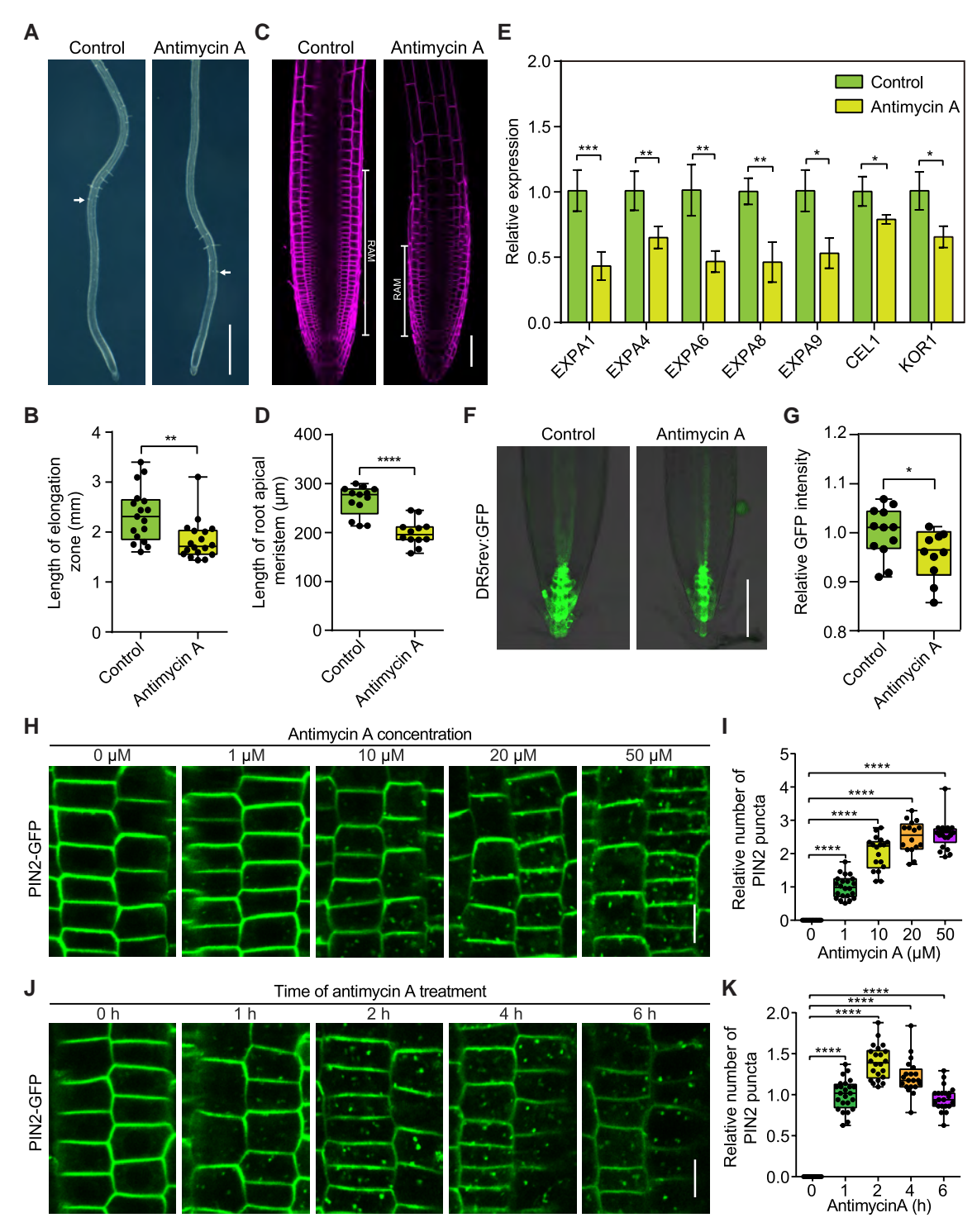


Figure 2. Antimycin A inhibits cell expansion and promotes PIN2 internalization. A) Length of the elongation zone (EZ) is reduced by AA. Five-d-old WT seedlings vertically grown on 1/2MS were transferred to 1/2 MS with dimethyl sulfoxide (DMSO) or AA (10  $\mu$ M) and grown vertically for 5 d. Arrows indicate the beginning of the root hair zone. Bar = 1 mm. B) Quantification of EZ length in A). Data are mean values  $\pm$  SD of >15 roots from three biological replicates. \*\*\*, P < 0.01, Student's t-test. C) Length of the root apical meristem (RAM) is reduced by AA. Seedlings in A) are stained with FM4-64 to outline cells. SAM region was marked by white flatheaded lines. Bar = 50  $\mu$ m. D) Quantification of RAM length in C). Data are mean values  $\pm$  SD of > 15 roots from three biological replicates. \*\*\*\*\*, P < 0.0001, Student's t-test. E) RT-qPCR of genes functioning in cell expansion in roots from A). Actin 2 was used as an internal control. Data are mean values  $\pm$  SD from one representative biological replicate (>10 roots) of three biological replicates. \*, P < 0.05; \*\*, P < 0.01; \*\*\*\*, P < 0.001, Student's t-test. F) GFP intensity of the auxin response marker DR5rev:GFP is reduced by AA. AA treatment was same as in A). Bar = 100  $\mu$ m. G) Quantification of GFP intensity in the columella in F). Data are mean values  $\pm$  SD from > 10 roots from three biological replicates. \*, P < 0.05, Student's t-test. H) PIN2 internalization following treatments of AA at different concentrations. Confocal images of epidermal cells in the root tip of PIN2-GFP after 2 h of AA treatment. Bar = 10  $\mu$ m. I) Quantification of cytoplasmic PIN2 puncta numbers per unit area in (H). Data are mean values  $\pm$  SD of > 15 cells from three biological replicates (>5 roots each). \*\*\*\*\*, P < 0.0001, Student's t-test. J) PIN2 internalization in a time course. Confocal images of epidermal cells in the root tip of PIN2-GFP treated with 20  $\mu$ M AA at indicated time points. Bar = 10  $\mu$ m. K) Quantification of cytoplasmic PIN2 puncta numbers per unit area in

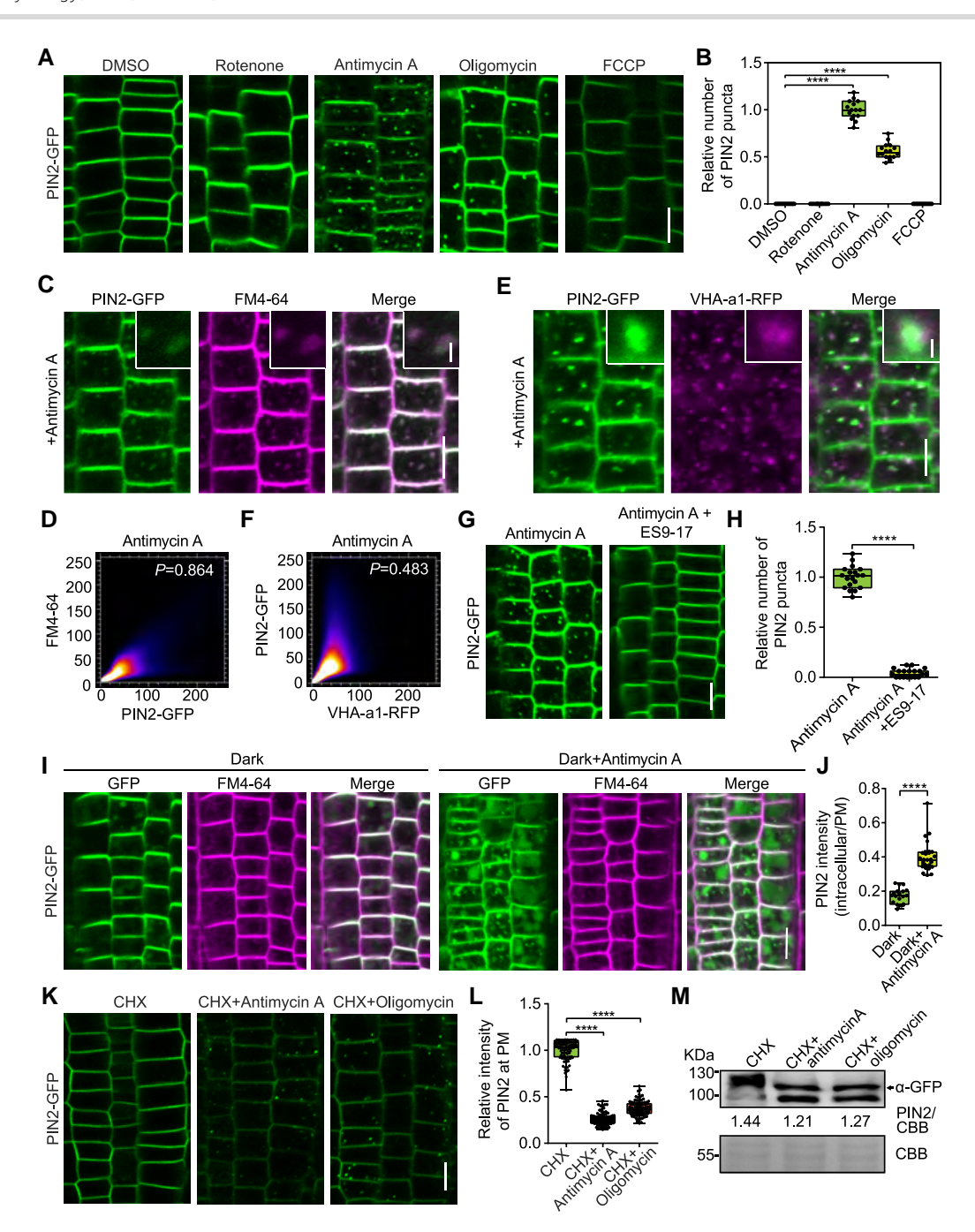


Figure 3. Antimycin A induces PIN2 endocytosis and vacuolar degradation. A) Effects of mETC inhibitors and uncoupler on PIN2-GFP sub-cellular distribution. Both AA and oligomycin promoted PIN2-GFP internalization. Rotenone had little effects on PIN2-GFP, whereas FCCP clearly reduced PIN2-GFP levels. B) Quantification of relative PIN2 puncta number in (I). Data are mean values ± SD of >15 cells from three biological replicates (>5 roots each). \*\*\*\*, P < 0.0001, Student's t-test. C) Co-localization of PIN2-GFP and FM4-64 2 h after 20 µM AA treatment in 5-d-old seedlings. FM4-64 staining was performed right before AA treatment. Bar = 10 μm. Insert, 5 x enlarged image, bar = 1 μm. D) Pearson's correlation coefficient graph for PIN2-GFP and FM4-64 signals in C). Significant co-localization was detected. E) Co-localization of PIN2-GFP and VHA-a1-RFP after 2 h of 20 µM antimycin A (AA) treatment in 5-d-old seedlings. Bar =  $10 \mu m$ . Insert,  $5 \times$  enlarged image, bar =  $1 \mu m$ . F) Pearson's correlation coefficient graph for PIN2-GFP and VHA-a1-RFP signals in E). Co-localization between PIN2 and VHA-a1 was not significant. G) AA-induced PIN2-GFP internalization is completely blocked by ES9-17, an endocytosis inhibitor. Five-d-old PIN2-GFP seedlings were treated with 20 µM AA alone, or 20 µM AA plus 50 µM ES9-17, for 2 h before imaging. Bar = 10 µm. H) Quantification of relative PIN2 puncta number in (G). Data are mean values ± SD of >25 cells from three biological replicates (>8 roots each). \*\*\*\*, P < 0.0001, Student's t-test. 1) AA accelerated dark-induced vacuolar accumulation of PIN2. Five-d-old PIN2-GFP seedlings pre-stained with FM4-64 were treated with dimethyl sulfoxide (DMSO) or AA in dark for 3 h. J) Quantification of intracellular/plasma membrane (PM) GFP intensity in 1). Data are mean values ± SD of >20 cells from three biological replicates (>8 roots each). \*\*\*\*, P < 0.0001, Student's t-test. K) Five-d-old PIN2-GFP seedlings were treated with the protein synthesis inhibitor cycloheximide (CHX, 100 µM), or with both CHX and AA or oligomycin (20 µM) for 2 h before imaging. AA and oligomycin further reduced PIN2-GFP intensity at the PM. L) Quantification of relative PIN2 intensity at the PM in (K). Data are mean values ± SD of >60 cells from three biological replicates (>10 roots each). \*\*\*\*, P < 0.0001, Student's t-test. M) AA and oligomycin promotes PIN2 degradation. Root tips of seedlings in K) were cut for membrane protein extraction and Western blotting (WB) detection of PIN2-GFP. Coomassie Brilliant Blue (CBB) staining of total protein served as loading control. PIN2 levels relative to CBB was quantified from a representative blot of three biological replicates. In B), H), J), and L), center lines, box range, whiskers, and points indicate the median, lower to upper quartile, 1.5 x interquartile, and statistical duplication, respectively.

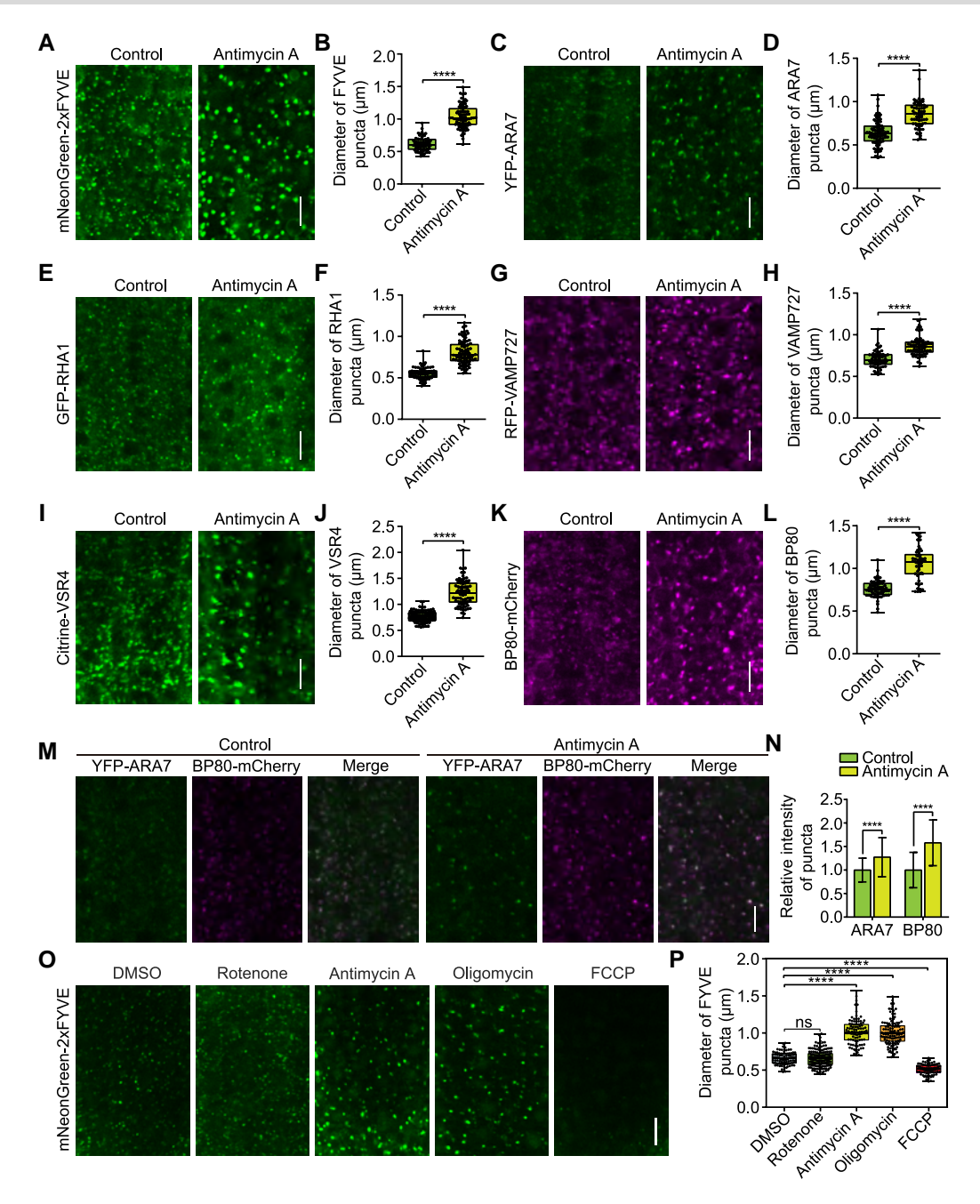


Figure 4. Multivesicular bodies are enlarged in AA-treated root cells. A) Accumulation of a PI3P probe mNeonGreen-2xFYVE after 2 h of 20 μΜ antimycin A (AA) treatment in 5-d-old seedlings. Bar = 10 µm. B) Quantification of FYVE puncta diameter, indicative of multivesicular bodies (MVBs) size, in A). Data are mean values ± SD of >60 cells from three biological replicates (>10 roots each). \*\*\*\*, P < 0.0001, Student's t-test. C) Confocal micrographs of root tip cells of 5-d-old YFP-ARA7 seedlings after dimethyl sulfoxide (DMSO) or 20 µM AA treatment for 2 h. Bar = 10 µm. D) Quantification of ARA7 puncta diameter, indicative of MVB size, in C). Data are mean values ± SD of >60 cells from three biological replicates (>10 roots each). \*\*\*\*, P < 0.0001, Student's t-test. E) Confocal micrographs of root tip cells of 5-d-old GFP-RHA1 seedlings after DMSO (control) or 20 µM AA treatment for 2 h. Bar = 10 µm. F) Quantification of RHA1 puncta diameter, indicative of MVB size, in E). Data are mean values ± SD of >60 cells from three biological replicates (>10 roots each). \*\*\*\*, P < 0.0001, Student's t-test. G) Confocal micrographs of root tip cells of 5-d-old RFP-VAMP727 seedlings after DMSO (control) or 20 µM AA treatment for 2 h. Bar = 10 µm. H) Quantification of VAMP727 puncta diameter, indicative of MVB size, in G). Data are mean values ± SD of >60 cells from three biological replicates (>10 roots each). \*\*\*\*, P < 0.0001, Student's t-test. I) Confocal micrographs of root tip cells of 5-d-old Citrine-VSR4 seedlings after DMSO (control) or 20 μM AA treatment for 2 h. Bar = 10 μm. )) Quantification of VSR4 puncta diameter, indicative of MVB size, in I). Data are mean values ± SD of >60 cells from three biological replicates (>10 roots each). \*\*\*\*, P < 0.0001, Student's t-test. K) Confocal micrographs of root tip cells of 5-d-old BP80-mCherry seedlings after DMSO (control) or 20 μM AA treatment for 2 h. Bar = 10 μm. L) Quantification of BP80 puncta diameter, indicative of MVB size, in (K). Data are mean values ± SD of >60 cells from three biological replicates (>10 roots each). \*\*\*\*, P < 0.0001, Student's t-test. M) AA-induced concurrent accumulation of ARA7 and BP80 in YFP-ARA7 BP80-mCherry double transgenic lines. Bar = 10 µm. N) Quantification of fluorescence intensity of ARA7 and BP80 in **M**). Data are mean values ± SD of >60 cells from three biological replicates (>10 roots each).
\*\*\*\*, P < 0.0001, Student's t-test. **O**) Effects of mETC inhibitors and uncoupler on the PI3P probe, mNeongreen-2xFYVE. Rotenone had little effects on PI3P; both AA and oligomycin induced enlargement of PI3P-labeled endosome, and FCCP reduced 2xFYVE levels. Bar = 10 µm. P) Quantification of sizes of PI3P-labeled endosomes in O). Data are mean values ± SD of >60 cells from three biological replicates (>10 roots each). ns, not significant, \*\*\*\*, P < 0.0001, Student's t-test. In B), D), F), H), J), L), and P), center lines, box range, whiskers, and points indicate the median, lower to upper quartile, 1.5 x interquartile, and statistical duplication, respectively.

PIN2, BOR1, PI3P, and TGN/EE and MVB/LE markers collectively suggested that inhibition of mETC promotes endocytosis of polar PM proteins functioning in cell elongation, and that the endocytosed PM proteins are partially stuck at enlarged MVB/LE.

# AA inhibits the RAB7 cycle and perturbs vacuole morphology maintenance

The enlarged MVB/LE with accumulated cargoes in AA-treated cells suggested that fusion of MVB with tonoplast is impaired. The Arabidopsis Rab7 homolog RABG3f localizes to MVB and the tonoplast membranes and is a key regulator of MVB-tonoplast fusion (Cui et al. 2014; Rodriguez-Furlan et al. 2019). As a Rab GTPase, RABG3f cycles between GTP-bound and active form and GDP-bound and inactive form. RABG3f Q67L (CA-RABG3f) corresponds to a constitutively active form, and RABG3f T22N (DN-RABG3f) corresponds to a dominant negative, inactive form (Cui et al. 2014). DN-RABG3f is known to localize to cytoplasm and endosome, whereas CA-RABG3f mainly localizes to the tonoplast (Cui et al. 2014). Moreover, overexpression of either CA-RABG3f or DN-RABG3f strongly changes vacuole morphology, resulting in rounded and fragmented vacuoles (Cui et al. 2014). We asked if AA can affect the level and distribution of RABG3f, and if such distribution is dependent on the activation state of RABG3f. AA treatment significantly promoted accumulation of GFP-RABG3f at MVB and on the tonoplast (Fig. 5, A to D; Supplementary Fig. S5, A to C), which is more like the localization pattern of CA-RABG3f (Fig. 5E; Supplementary Fig. S5A). These observations suggested that RABG3f is stuck in the GTP-bound form and accumulated on MVB and, especially, the tonoplast.

We then examined vacuole morphology in response to AA treatment with a line carrying YFP-VAMP711, a v-SNARE that localizes to tonoplast, and 7-amino-4-chloromethylcoumarin (CMAC), a fluorescent dye that stains the vacuole lumen (Wang et al. 2023). Vacuoles became fragmented and spherical after AA treatment (Fig. 5, H to J). We documented the time course of changes in vacuole morphology, and spherical vacuoles were already prominent 2 h after AA treatment in the entire root tip, except for some large epidermal cells (Supplementary Fig. S5, D and E, Supplementary Videos S1 and S2).

To further establish the causal relationship between mitochondrial dysfunction and changes in vacuole morphology, we collected several mitochondrial mutants with reported dysfunction and developmental defects, including ndufs4, ftsh4, and lon1-1. NDUFS4 encodes the NADH dehydrogenase (ubiquinone) fragment S subunit 4 (Meyer et al. 2009), FtSH4 encodes an inner membrane-bound mitochondrial AAA-protease (Gibala et al. 2009; Zhang et al. 2014a, 2014b), and LON1 encodes a multifunctional ATP-dependent protease (Rigas et al. 2009). All three mutants have fragmented and spherical vacuoles when grown on ½ MS, mimicking AA-treated wild-type seedlings. We concluded that changes in vacuole morphology are a result of mitochondrial dysfunction.

# AA strongly affects Golgi structure and localization of Golgi SNAREs

When imaging PIN2-GFP after AA treatment, we noticed that, apart from accumulating in cytoplasmic puncta, PIN2 at the PM dwindled within several hours (Fig. 2, H and J; Fig. 3G), which is not prevented by ES9 treatment (Fig. 3G). We quantified the relative intensity of PIN2 at the PM and found out it reduced within 2 h of AA treatment (Fig. 6, A and B). A similar reduction was observed for BOR1 (Supplementary Fig. S6, A and B). Such observation indicated that some newly synthesized PIN2 and BOR1 might be stuck in the secretory pathway. To see which organelle along the secretory pathway may be affected by AA, we examined the Golgi, ERGIC, and the ER.

TEM showed that the Golgi apparatus loses its overall structure upon AA treatment (Fig. 6C), possibly a consequence of decreased actin polymerization due to ATP depletion. We selected three markers to dissect the possible Golgi defects caused by AA, including the cis-Golgi Qa-SNARE SYP32 (Uemura et al. 2004; Rui et al. 2021) and the Qb-SNARE MEMBRIN12 (MEMB12) (Uemura et al. 2004; Fougère et al. 2023), and a trans-marker ST-GFP, a signal anchor sequence of a rat sialyl transferase fused with GFP (Saint-Jore et al. 2002). We also generated several double transgenic lines carrying these Golgi markers and TGN markers.

Upon AA treatment, MEMB12 completely lost its Golgi localization (Fig. 6, D and E; Supplementary Videos S3 and S4). In a transgenic line carrying both MEMB12-RFP and GFP-SYP32, AA treatment led to re-localization of both MEMB12 and SYP32 to a perinuclear network that appears to be the ER, and SYP32 partially maintained its Golgi localization pattern (Fig. 6F; Supplementary Fig. S6, C and D). Like SYP32, ST-GFP partially maintained its Golgi localization (Supplementary Fig. S6, E and F), and partially co-localized with MEMB12 in perinuclear, ER-like structures after AA treatment (Supplementary Fig. S6G). Such observation agrees with the TEM results, in which Golgi structure is severely affected but still visible, since SYP32, like SYP31, is a core component of the cis-Golgi, and ST marks the trans-Golgi, whereas MEMB12 is believed to localize not only to cis-Golgi, but is a component of the recently identified ER-Golgi Intermediate Compartment (ERGIC) in Arabidopsis (Fougère et al. 2023), through which some ER-to-Golgi cargoes pass. We further examined how other mETC inhibitors and uncoupler affect MEMB12 localization, and again found out oligomycin and AA had similar strong effects, and that rotenone had limited effect on MEMB12. FCCP, however, appeared to affect MEMB12 less than AA and oligomycin (Fig. 6, G and H). This is reasonable because, as an uncoupler, FCCP should primarily affect compartments with delta pH; however, H<sup>+</sup>-ATPase is not known to be present in the ERGIC.

To see whether AA can affect the spatial relationship between the Golgi and ERGIC and TGN/EE, transgenic lines carrying MEMB12-RFP/ GFP-SYP43 were analyzed. As shown in Supplementary Fig. S6H, co-localization between MEMB12-RFP and GFP-SYP43, a TGN/EE marker, were reduced by AA, mainly because MEMB12 largely re-localized to perinuclear, ER-like structures (Supplementary Fig. S6H).

# BFA compartments were much smaller in the presence of AA likely due to reduced Golgi number

We further confirmed AA-induced reduction in Golgi number by treating cells with Brefeldin A (BFA). BFA binds to the interface between the GTPase ARF and its GEF (Mossessova et al. 2003) and reversibly inhibits ER-Golgi protein trafficking. It causes redistribution of Golgi resident proteins into the ER and induces formation of BFA bodies, which are formed by multiple Golgi stacks and surrounding TGN/EE vesicles. We postulated that reduced Golgi number would cause reduced size of BFA bodies. Indeed, BFA bodies containing PIN2-GFP and stained by FM4-64 were much smaller in the presence of AA (Fig. 7, A and B). Likewise, auxin flux carriers PIN1-GFP and AUX1-GFP accumulated less in much smaller compartments (Supplementary Fig. S7, A to D). TGN/EE markers, GFP-SYP43 and VHA-a1-GFP, and vacuolar sorting receptors, Citrine-VSR4 and BP80-mCherry, all gave similar results (Fig. 7, C to F; Supplementary Fig. S7, E to H). Lastly, in a double

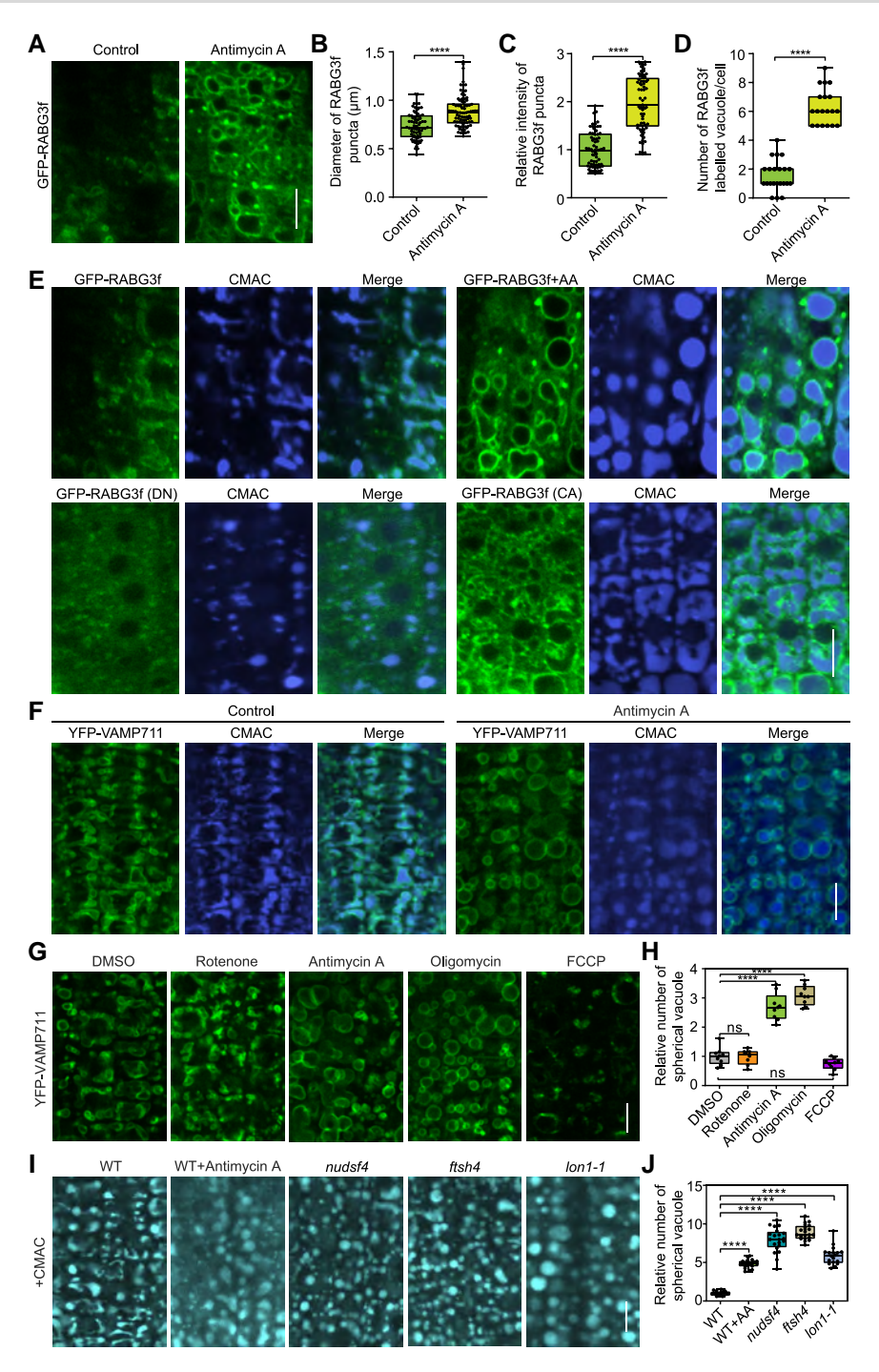
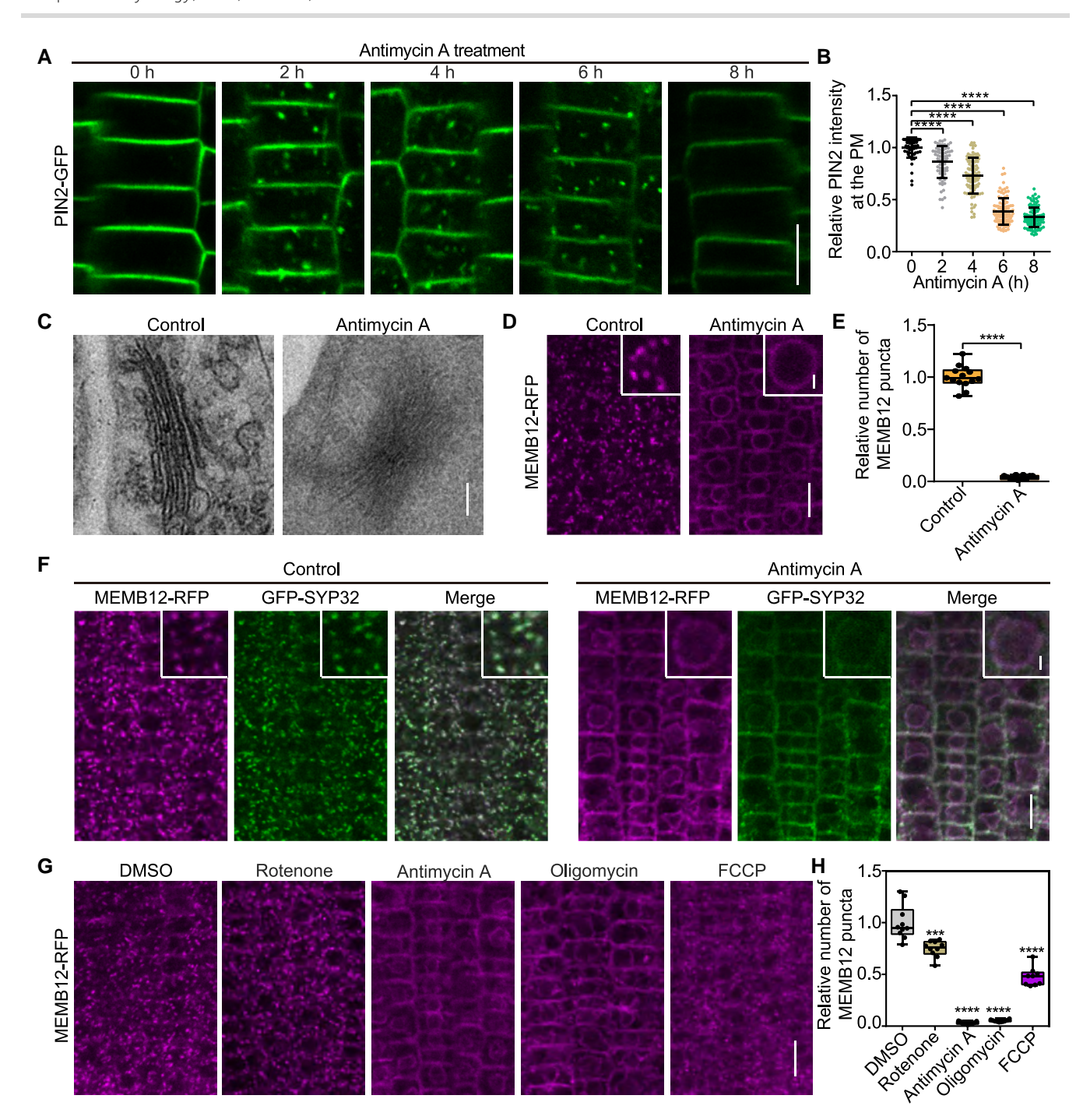


Figure 5. Antimycin A induces RABG3f accumulation on tonoplast and changes vacuole morphology. A) GFP-RABG3f accumulated on tonoplast after antimycin A (AA) treatment. Confocal micrographs of GFP-RABG3f root tip cells 2 h after dimethyl sulfoxide (DMSO) or 20 µM AA treatment. Bar = 10 µm. B) Quantification of RABG3f puncta diameter, indicative of MVB size, in A). Data are mean values ± SD of >60 cells from three biological replicates (> 10 roots each). \*\*\*\*, P < 0.0001, Student's t-test. C) Quantification of relative intensity of RABG3f puncta, indicative of amount of RABG3f at MVB, in A). Data are mean values ± SD of >60 cells from three biological replicates (> 10 roots each). \*\*\*\*, P < 0.0001, Student's t-test. D) Quantification of RABG3f-labeled vacuole numbers per cell in A). Data are mean values ± SD of >60 cells from three biological replicates (> 10 roots each). \*\*\*\*, P < 0.0001, Student's t-test. E) Comparison of RABG3f sub-cellular localization in WT form (both with or without AA), GTP-bound form (Q67L, constitutively active, CA), and GDP-bound form (T22N, dominant negative, DN). RABG3f treated with AA is very similar to RABG3f Q67L. Vacuoles were pre-stained with CMAC for 30 min before imaging. Bar = 10 µm. F) Altered vacuole morphology after AA treatment. YFP-VAMP711 root tip cells were imaged 2 h after DMSO (control) or 20 µM AA treatment. Vacuoles were pre-stained with CMAC for 30 min before imaging. Bar = 10 µm. G) Effects of mETC inhibitors and uncoupler on vacuole shape, outlined by YFP-VAMP711. Rotenone had little effects; both AA and oligomycin treatments led to spherical and fragmented vacuoles, and FCCP reduced YFP-VAMP711 levels. Bar = 10 µm. H) Quantification of relative number of spherical vacuoles in regions of a same size in **G**). More than 8 roots from 3 biological replicates were used for quantification. ns, not significant; \*\*\*\*, P < 0.0001, Student's t-test. I) Mutants with mitochondrial dysfunction also exhibit abnormal vacuolar morphology. Root tip cells of wild-type (WT), WT treated by 20 μM AA, ndufs4, ftsh4, and lon1-1 mutant were imaged after CMAC staining of the vacuole. Bar = 10 µm. )) Quantification of relative number of spherical vacuoles in regions of a same size in (I). More than 8 roots from 3 biological replicates were used for quantification. \*\*\*\*, P < 0.0001, Student's t-test. In B), C), D), H), and J), center lines, box range, whiskers, and points indicate the median, lower to upper quartile, 1.5 x interquartile, and statistical duplication, respectively.



transgenic line carrying YFP-ARA7 and VHA-a1-RFP, both ARA7 and VHA-a1-RFP co-localized to these smaller compartments after BFA plus AA treatment (Supplementary Fig. S7I).

To see how the spatial relationship between Golgi and TGN/EE may change in response to AA plus BFA, we treated double transgenic lines carrying MEMB12-RFP/GFP-SYP43 and GFP-SYP32/

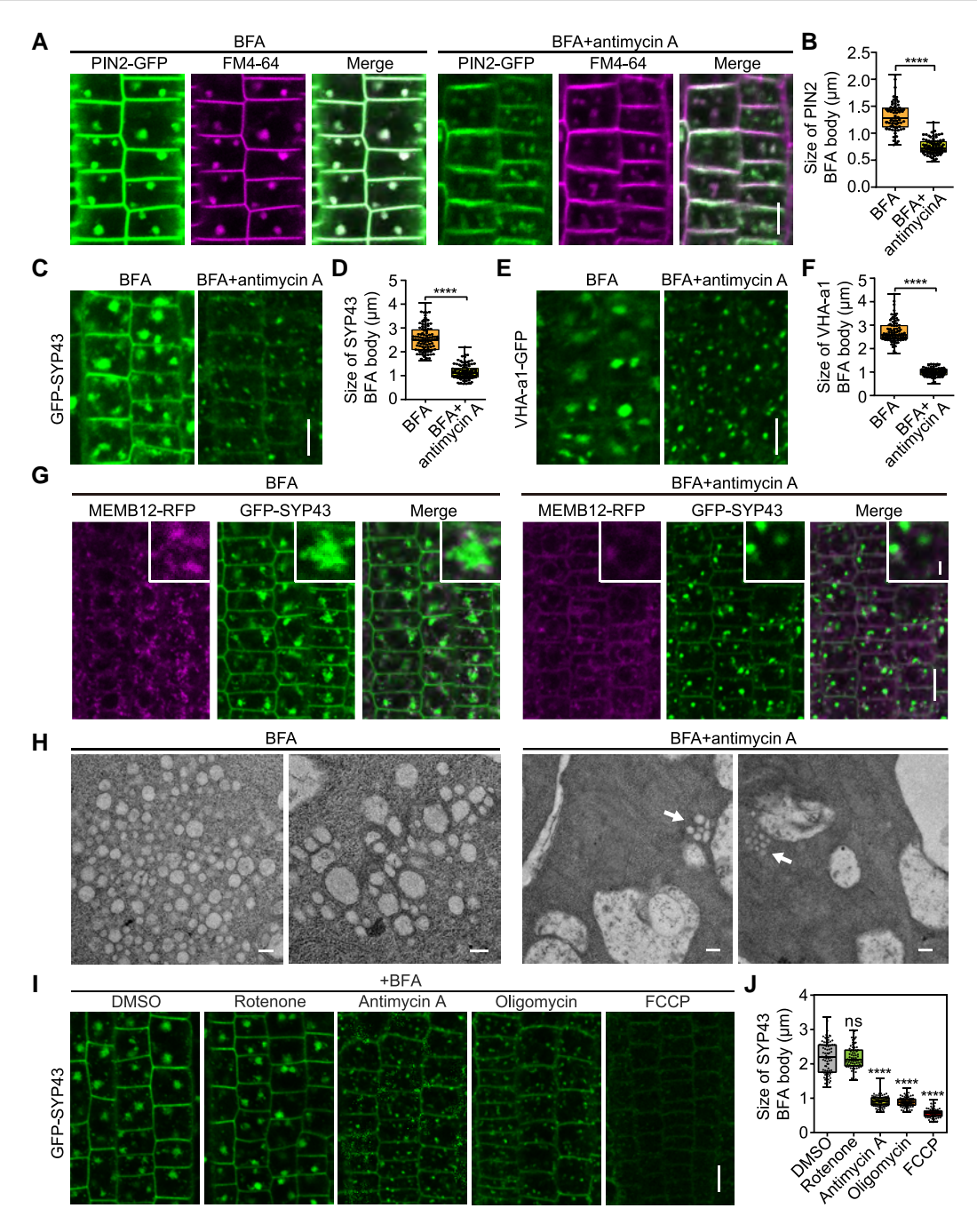


Figure 7. Formation of BFA bodies is compromised in antimycin A-treated cells. A) Brefeldin A (BFA) bodies, indicated by PIN2-GFP, are smaller in antimycin A (AA)-treated cells. Five-d-old PIN2-GFP seedlings, pre-stained with FM4-64, were treated with dimethyl sulfoxide (DMSO) or 20 µM AA for 2 h. BFA (50 μM) was added for another 1 h before imaging. Bar = 10 μm. B) Quantification of the diameter of BFA bodies in A). Data are mean values ± SD of >60 cells from three biological replicates (>10 roots each). \*\*\*\*, P < 0.0001, Student's t-test. C) BFA bodies, indicated by GFP-SYP43, are smaller in AA-treated cells. Five-d-old GFP-SYP43 seedlings were treated with DMSO (control) or 20 µM AA for 2 h. BFA (50 µM) was added for another 1 h before imaging. Bar = 10 µm. D) Quantification of the diameter of BFA bodies in C). Data are mean values ± SD of >60 cells from three biological replicates (>10 roots each). \*\*\*\*, P < 0.0001, Student's t-test. E) BFA bodies, indicated by VHA-a1-GFP, are smaller in AA-treated cells. Five-d-old VHA-a1-GFP seedlings were treated with DMSO (control) or 20 μM AA for 2 h. BFA (50 μM) was added for another 1 h before imaging. Bar = 10 μm. F) Quantification of the diameter of BFA bodies in E). Data are mean values ± SD of >60 cells from three biological replicates (>10 roots each). \*\*\*\*, P < 0.0001, Student's t-test. G) Reduced sizes of BFA bodies are due to loss of endoplasmic reticulum-Golgi intermediate compartment (ERGIC) and trans-Golgi network or early endosome (TGN/EE). Five-d-old double transgenic seedlings carrying MEMB12-RFP and GFP-SYP43 were treated with DMSO (control) or 20 µM AA for 2 h. BFA (50 µM) was added for another 1 h before imaging. BFA bodies are composed of TGN/EE vesicles, surrounded by Golgi and ERGIC. Both parts are reduced in size and fluorescent intensity in the presence of AA. Bar =  $10 \, \mu m$ . Insert,  $3 \times$  enlarged image, bar =  $2 \, \mu m$ . H) TEM images of BFA compartments with or without AA. Root tips of 5-d-old WT seedlings were treated with DMSO (control) or 20 μM AA for 2 h, and BFA (50 μM) was added for another 1 h before fixation. Bar = 200 nm. White arrows indicate BFA bodies that are greatly reduced in size. 1) Effects of mETC inhibitors and uncoupler on BFA bodies, indicated by GFP-SYP43. All drugs except for rotenone significantly reduced sizes of BFA bodies. I) Quantification of the diameter of BFA bodies in 1). Data are mean values ±SD of >60 cells from three biological replicates (>10 roots each). ns, not significant; \*\*\*\*, P < 0.0001, Student's t-test. In B), D), F) and G), center lines, box range, whiskers, and points indicate the median, lower to upper quartile, 1.5 x interquartile, and statistical duplication, respectively.

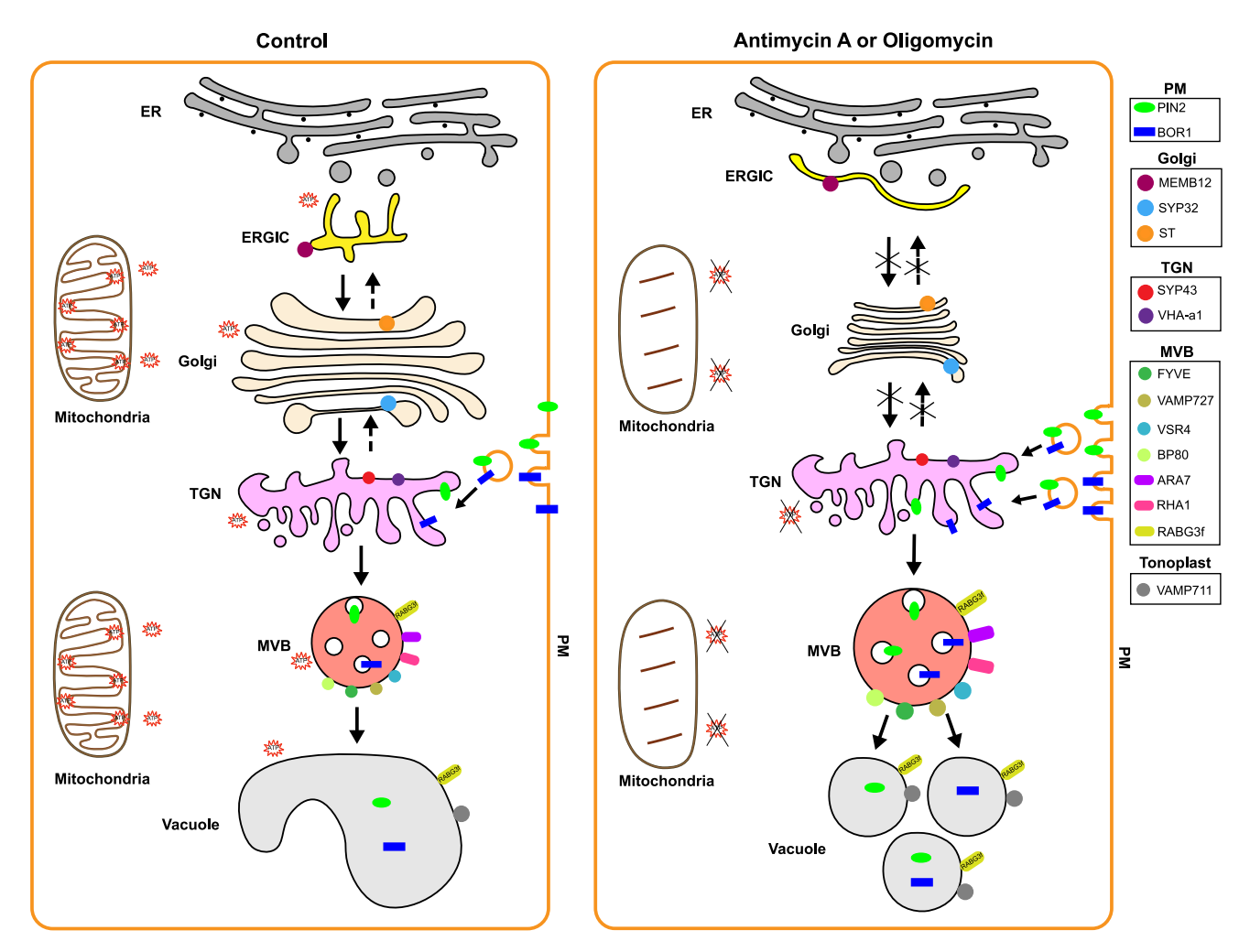


Figure 8. A model that summarizes our findings. Antimycin A (AA) inhibits mitochondrial electron transport chain (mETC) to reduce ATP production and impairs mitochondrial morphology. The endomembrane system and intracellular trafficking are severely affected by AA. The trans-Golgi network/early endosome (TGN/EE) is the only vesicle population free from morphological changes. Starting from TGN/EE, toward the vacuole, plasma membrane (PM)-localized membrane proteins functioning in cell expansion, such as PIN2 and BOR1, are partially stuck at enlarged multivesicular bodies or late endosome (MVB/LE). Fusion between MVB/LE and the vacuole is inhibited and the vacuole becomes spherical and fragmented. The Rab7 homolog, RABG3f, is trapped at the tonoplast likely in a GTP-bound form. In the other direction, neither the Golgi apparatus nor the ERGIC can be maintained; proteins functioning in the Golgi and especially the endoplasmic reticulum—Golgi intermediate compartment (ERGIC) are relocated to the endoplasmic reticulum (ER). Accelerated endocytosis and eventually degradation of PIN-FORMED 2 (PIN2) and REQUIRES HIGH BORON 1 (BOR1) lead to reduced cell expansion and short root phenotype in AA-treated seedlings.

VHA-a1-RFP with BFA or BFA plus AA. As expected, BFA alone led to accumulation of MEMB12-RFP around aggregated GFP-SYP43; AA plus BFA greatly reduced the size of BFA compartments labeled by GFP-SYP43, whereas MEMB12-RFP redistributed into the ER (Fig. 7G). Same localization patterns were observed for GFP-SYP32 and VHA-a1-RFP (Supplementary Fig. S7J). TEM further validated the reduced size of BFA compartment, in which the TGN/EE vesicles were greatly reduced in number and sizes (Fig. 7H).

We also compared the effects of the inhibitors of mitochondrial functions on BFA compartment formation. Again, AA and oligomycin affected BFA compartment in similar ways, rotenone had little effect, and FCCP greatly reduced accumulation of SYP43 and PIN2 (Fig. 7, I and J; Supplementary Fig. S7, K and L). We summarize our findings in a model to illustrate how the endomembrane system responds to mitochondrial mETC inhibitors and uncouplers in a hierarchy of events that occurs upon cellular energy depletion (Fig. 8).

## Discussion

The relationship between mitochondria and the endomembrane system has a deep root in evolution. The emergence of the endomembrane system is believed to be one of the great changes brought by the endosymbiosis of an archaea and an alphaproteobacteria, which is the ancestor of mitochondria. It can be postulated that mitochondria activities are essential in maintaining such highly dynamic and energy-consuming entities in today's cells; however, in our knowledge, such experimental evidence is limited for plant cells. This study therefore aimed at providing a relatively detailed description of how inhibition of mitochondrial energy production can actually affect the form and function of the endomembrane system.

On our hands, oligomycin and antimycin A have similar impacts on endomembrane organelles and vesicle trafficking, rotenone is not so effective since plants have additional NADH dehydrogenases, and the decoupler/ionophore FCCP had the

strongest effect, likely because it abolishes proton/ion gradients across membranes. The imaging results are in general consistent with the ATP levels indicated by the ATP biosensor AT1.03 (Fig. 1).

An interesting finding here is that the TGN/EE appears to be the only organelle/vesicle population in the endomembrane system that does not change in morphology; it only became dim due to decreased protein levels (Fig. 4; Supplementary Fig. S4). This observation agrees with what we know about TGN/EE; ATP or GTP consumption in large quantities had not been described for this organelle before, although V-ATPase activity in the TGN/EE was shown to be required for secretion and protein (re)cycling in Arabidopsis aside of vacuolar acidification (Luo et al. 2015). In contrast, vesicle budding from the ER, clathrin-mediated endocytosis, homotypic fusion of vacuoles, and fusion of MVB/LE to vacuoles, all consume large amounts of ATP or GTP. Apart from H<sup>+</sup>-ATPases that establish proton gradients that drives secondary transport across the PM and the tonoplast, which are critical in cellular homeostasis, the places where AAA-ATPase is required are also presumably very energy consuming. These included the release of used SNARE from target vesicles, including tonoplast, by the AAA-ATPase NSF; the formation of intraluminal vesicles in MVB, in which the AAA-ATPase VPS4/SKD1 cuts the membrane, and the ERAD and CHLORAD, in which the AAA-ATPase CDC48 is used for pulling out ubiquitinated protein from the ER or the chloroplast. CDC48 also functions in the recycling of peroxisomal import receptors such as peroxin 5 (PEX5). Our observation on retardation in MVB-vacuole fusion is consistent with the idea of energy consumption. Nevertheless, whether these steps are truly critical in determining the form of function of endomembrane system in response to energy depletion needs more direct evidence.

Another interesting finding is that AA can induce significant changes in vacuole morphology: the lytic vacuole became fragmented and rounded. Similar vacuole morphology were observed in several mutants with defective mitochondrial functions (Fig. 5), thus validating a link between dysfunctional mitochondria with failure in maintaining vacuole morphology. There are several plausible explanations. First, actin cytoskeleton is involved in vacuole morphology (Zhang et al. 2014a, 2014b), and actin polymerization and bundling processes are highly energy consuming. Second, upon AA treatment, the key Rab GTPase at MVB/LE and vacuole, Rab7, can be seen localized mainly at the tonoplast (Fig. 5; Supplementary Fig. S5), resembling the localization pattern of GTP-bound Rab7 (RABG3F-CA). We further found that RABG3F(CA) and AA-treated RABG3F segregated into vesicles of same densities upon sucrose density gradient centrifugation, and RABG3F(CA) seedlings are less sensitive to AA treatment (Fig. 5; Supplementary Fig. S5). Rab GTPases cycle between GTP-bound and GDP-bound forms with the aid of GEF and GAP proteins, and upon activation they recruit downstream effectors to organize trafficking routes, such as endosome maturation and fusion events between endosomes and vacuoles (Takemoto et al. 2018; Minamino and Ueda 2019). Interrupting the Rab7 cycle can certainly impair MVB/LE and vacuole fusion. A recent report showed that NETWORKED 4 (NET4) proteins that bind to F-actin and localize to the vacuole to mediate actin-vacuole interactions are RABG3 effectors (Hawkins et al. 2023). Whether RABG3-NET4 interaction, and subsequently, actin bundling on the vacuole, would be interrupted by AA treatment, or mitochondrial dysfunction, is unknown. The fragmented vacuole phenotypes have also been documented in zig-1 and vti11 alleles of the vacuolar/ MVB Qb-SNARE VTI11 (Ebine et al. 2014; Zheng et al. 2014). Importantly, the quintuple rabq3b,c,d,e,f mutation (rabq3) suppressed the short inflorescence phenotype of zig-1 (Ebine et al.

2014), and treating vti11 with PI3K inhibitors wortmannin and LY294002 induced vacuole fusion in the mutant (Zheng et al. 2014). These observations indicated that over-accumulation of PI3P at the MVB, rather than timely turnover inside the vacuole (Kim et al. 2001), may lead to constitutive activation of Rab7 and subsequently, inhibition of vacuole fusion or activation of vacuole fission. Last, in animal cells, mitochondria-lysosome membrane contact formation is promoted by GTP-bound lysosomal Rab7 to mark mitochondrial fission sites, and such contacts allow bidirectional regulation of mitochondrial and lysosomal dynamics (Wong et al. 2018). In addition, damaged mitochondria also undergo various forms of autophagy including microautophagy, and such processes may also require Rab7 activity, since Rab7 and its downstream effectors are key players in homotypic fusion of vacuoles and fusion of vacuoles with MVBs (Hao et al. 2016; Takemoto et al. 2018; Rodriguez-Furlan et al. 2019). Whether similar mitochondria-vacuole contact may exist in plant cells and play a role in vacuole morphology awaits further exploration.

AA-induced short root phenotype can be explained by the alkalinization of the extracellular matrix. Cell wall acidification triggers cell wall loosening to allow for cell expansion, for cell wall-loosening enzymes are activated by low pH (Cosgrove 2015). Apart from the fact that depletion or less proton pumping at the PM results in alkalinization of the apoplast, similar to the effect of rapid alkalinization factor (RALF) peptides via receptorlike kinase FERONIA-mediated phosphorylation of AHA2 (Haruta et al. 2014; Cheung 2024). Genes functioning in cell expansion are down-regulated, and exogenous ATP can induce their expression in the presence of AA (Fig. 2; Supplementary Fig. S2). Also, auxin response at the root tip is down-regulated, likely due to reduced basipetal transport of auxin toward the RAM. On the other hand, PIN2, the key auxin efflux carrier in EZ establishment, is actively endocytosed for vacuolar degradation (Figs. 2 and 3; Supplementary Fig. S2). It is noteworthy that many studies have, through genetic screens, chemical genetic screens, reverse genetics, and transcriptome analyses, established the relationship between mitochondrial dysfunction and auxin signaling (Ivanova et al. 2014; Kerchev et al. 2014; Berkowitz et al. 2016; Ohbayashi et al. 2019; Tivendale et al. 2021; Tivendale and Millar 2022). Here we mainly used PIN2 as a marker protein that undergoes endocytosis and functions in cell expansion. Another key protein in cell expansion, BOR1, is also actively endocytosed for vacuolar degradation (Supplementary Figs. S2 and S3). The fact that endocytosis is enhanced during stress may be related to altered cell wall mechanics resulting from changes in the pectin methylesterification state, which stimulates RALF-FER signaling. In general, activation of FER and reduced proton pumping into the apoplast may lead to alkalinization of the apoplast (Cheung 2024). Furthermore, it has been revealed that the mitochondrial uncoupler ES9 and the endocytosis inhibitor Tyrphostin A23 actually block clathrin-mediated endocytosis by promoting acidification of the cytoplasm (Dejonghe et al. 2016), thus the accelerated endocytosis of PIN2 and BOR1 are active instead of passive. We also showed that ES9 can block AA-induced PIN2 endocytosis (Fig. 3). All these observations suggested that root growth in Arabidopsis is shut down upon energy deficiency.

During this process, reduced ER-to-Golgi trafficking leads to an imbalance in Golgi stacking, eventually reduces Golgi numbers and sizes. The involvement of ERGIC in this process is also evident, since MEMB12, the ERGIC marker, completely relocated to the ER after AA treatment (Fig. 6; Supplementary Fig. S6). Using BFA as a tool, and by showing that BFA bodies became tiny with very few TGN/EE vesicles, we further demonstrated how AA affects Golgi

numbers and sizes (Fig. 7; Supplementary Fig. S7). Such depletion of protein trafficking is striking and reflects the importance of energy production in maintaining membrane trafficking. Alternatively, disruption of the cytoskeleton, especially energy-consuming actin polymerization, may also explain the reduction in Golgi numbers and sizes.

In summary, our study described how the endomembrane system responds to mitochondrial mETC inhibitors and uncouplers that lower pH gradients over membranes, revealing a hierarchy of events affected by cellular ATP depletion. This study opens many questions on how signals are produced by the dysfunctional mitochondria and how they are sensed and transduced by the individual organelles in the endomembrane system. Meanwhile, it paves the way for future studies on the interactions between energy-producing organelles and energy-consuming organelles, and may help us in understanding cellular behavior from a new angle.

# Materials and methods

# Plant materials and growth conditions

MEMB12-RFP was a gift from Dr. Yiqun Bao. BOR1-GFP, GFP-SYP32, and ST-GFP were a gift from Dr. Caiji Gao. AT1.03 was a gift from Dr. Boon Leong Lim. PIN2-GFP was a gift from Dr. Ben Scheres and Dr. Shuzhen Men, VHA-a1-GFP and VHA-a1-RFP, and TagRFP-VAMP727 were a gift from Quan-Sheng Qiu. Citrine-VSR4 was a gift from Dr. Nadine Paris. Mito-GFP (3xHA-eGFP-OMP25) was a gift from Dr. Hong Yu. DR5rev: GFP, AUX1-YFP, PIN1-GFP, YFP-ARA7, and YFP-VAMP711 were obtained from ABRC. ftsh4, ndufs4 and lon1-1 mutants were gifts from Drs. Shengchun Zhang, Chengwei Yang, Xu Wang, and Lei Li. All double transgenic lines were generated by crossing and confirmed by fluorescent microscopy.

Generally, Arabidopsis thaliana (ecotype Columbia-0, Col-0) seeds were surface-sterilized with 75% ethanol for 5 min, rinsed with ddH<sub>2</sub>O for five times, then stratified at 4 °C for 2 d before plated on 1/2 Murashige and Skoog (1/2 MS) medium (Duchefa, Netherland) containing 0.8% (w/v) agar, 1% (w/v) sucrose, pH 5.7. The plants were then kept at a 16 h light (22 °C)/8 h dark (18 °C) photoperiod with a photosynthetic photon flux density at 120  $\mu\text{E}~\text{m}^{-2}~\text{s}^{-1}$  in a growth room. Soil-grown plants were kept under the same conditions.

# Plasmid construction

For stable transformation, genomic DNA or full length cDNAs were fused in-frame with GFP and mCherry tags under the control of endogenous or UBQ10 promoter, in modified pCAMBIA vectors to generate GFP-SYP43, GFP-RHA1 and BP80-mCherry. DN (T22N) or CA (Q67L) form of RABG3f was generated by recombination of two PCR fragments, one containing PCR products carrying the corresponding point mutation, the other containing the rest of the cDNA, using a homologous recombination kit (Vazyme, C112-02). Constructs were verified by DNA sequencing. Primers used are listed in Supplementary Table S1.

# Plant transformation

To generate Arabidopsis transgenic lines, constructs were introduced into Agrobacterium tumefaciens (GV3101) for floral dipping (Clough and Bent 1998). Primary transformants were selected by antibiotic resistance and further verified by PCR and fluorescent microscopy. Individual T2 and T3 lines were used.

# Reverse transcription quantitative PCR

RNA extraction, reverse transcription, and reverse transcription quantitative PCR (RT-qPCR) were done as described (Wang et al. 2023). The relative expression of target genes were analyzed by  $2^{-\Delta\Delta Ct}$  methods and expression of control was normalized to 1. ACTIN2 (AT3G18780) was used as the internal control. Primers used are listed in Supplementary Table S1.

# Drug treatment

To measure additional root growth on antimycin A, 5-d-old vertically grown Col-0 seedlings were transferred to new 1/2 MS plates containing different concentrations of antimycin A, or to 1/2 MS plates containing dimethyl sulfoxide (DMSO) and grown for 7 or 9 d. Similarly, ATP (0.5 or  $1 \mu M$ ) was added to the plates to document additional root growth on AA plus ATP. For auxin-related observations, 5-d-old vertically grown seedlings carrying DR5rev: GFP or PIN2-GFP were transferred to ½ MS medium containing 10 μM of antimycin A and grown for another 5 d. For the observation of protein localization influenced by antimycin A, 5-d-old seedlings carrying various fluorescent protein-tagged marker genes were immersed in liquid ½ MS medium containing AA or DMSO control for different periods of time, before confocal imaging. For observation of mitochondria membrane depolarization, 5-d-old seedlings were stained with 100 nm of MitoTracker or TMRE for 30 min after treated with DMSO or antimycin A for 2 h. For viability staining, seedlings were stained with fluorescein diacetate (FDA, 5 µg/mL) and PI (10 µg/mL) for 5 min before confocal imaging. For PM staining and pulse chase of endocytosis, 5-d-old seedlings were incubated in liquid ½ MS media with 2 µM of FM4-64 on ice in the dark for 7 min before FM4-64 washout. For observation of BFA compartments, 5-d-old seedlings were pretreated with 100  $\mu M$  of CHX for 1 h, followed with DMSO or 20  $\mu M$ of antimycin A treatment. Brefeldin A (BFA) (50 µM) was added to the solution for another 1 h before confocal imaging. For observation of vacuoles in root tip cells, 5-d-old seedlings treated with liquid 1/2 MS media containing DMSO or antimycin A were stained with  $1\,\mu\text{M}$  of CMAC for 15-30 min. For treatment of each mitochondria ETC inhibitor or decoupler, 5-d-old seedlings carrying AT1.03, PIN2-GFP, BOR1-GFP, mNeonGreen-2xFYVE, BP80-mCherry, mRFP-VAMP727, YFP-VAMP711, MEMB12-RFP, and GFP-SYP43 were immersed in liquid 1/2 MS media with a same concentration  $(20 \mu M)$  of drug for 2 h.

## Confocal microscopy

For observation of root EZ, 5-d-old Col-0 seedlings were transferred to solid 1/2 MS media containing DMSO or 10 μM of antimycin A for 5 d. The EZ of primary roots was photographed under a stereoscope (M205 FA, Leica, Germany). For observation of root meristematic zone, the primary roots stained by FM4-64 were photographed on a confocal microscope (Ni-E A1 HD25 confocal microscope, Nikon, Japan). All other confocal images were also captured with this confocal microscope. GFP, YFP, and Citrine were exited at 488 nm and emission collected at 500 to 550 nm. mCherry and RFP were exited at 561 nm and collected at 570 to 620 nm. The FM4-64 fluorescence was exited at 561 nm and collected at 620 to 650 nm. The CMAC and DAPI fluorescence were exited at 405 nm and collected at 435 to 485 nm. To compare the intensity of fluorescent proteins with or without treatments, the observation parameters on the microscope were set as the same for control and experimental group. The MitoTracker or TMRE fluorescence were exited at 550 nm and collected around 570 nm. The ATP sensor AT1.03 was excited at 445 nm and its emission

was collected from 470 to 507 nm (CFP image) and from 526 to 545 nm (Venus image).

# Statistical analysis

The primary root length of Arabidopsis seedlings, fluorescence intensity of protein expression and co-localization of two proteins were counted and measured by Image J. The differences between samples was calculated by Student's t-test (unpaired and two-tailed) using SPSS, and P-value less than 0.05 was defined as with significant difference (\*, P < 0.05; \*\*, P < 0.01; \*\*\*, P < 0.001; \*\*\*\*, P < 0.0001). All experiments were replicated at least three times, and representative data from the independent experiments were shown. Bar charts and box plots were plotted with GraphPad Prism 8, and figures were assembled with Adobe Illustrator CS6.

# Sucrose density gradient centrifugation

About 100 mg of 7-d-old transgenic seedlings were mixed with  $200\,\mu L$  of KHE buffer (1 mm DTT, 0.4 m sucrose, 10 mm KAc, 50 mm HEPES and 1 mm EDTA, the pH was adjusted to 7.5 by KOH and 0.1 mm PMSF was added before use). The mixture was centrifuged for 10 min at 12,000 rpm to collect the supernatant. 54%, 40%, 33%, 24%, and 15% sucrose (W/V) and the supernatant were added to a 2 mL high-speed centrifuge tube in sequence, and the volumes of the six components are 212.77  $\mu$ L, 574.5  $\mu$ L, 468  $\mu$ L, 425.5 μL, 160 μL, and 160 μL, respectively. Centrifuge with 150, 000 g for 4 h at 4 °C. The centrifuged sucrose solution was pipetted out from top to bottom in 14 layers (140 µL of sample from each layer), and the samples were boiled with 5 x SDS loading buffer at 100 °C for 5 min before western blotting.

# Western blotting

For detecting of protein levels of PIN2 and BOR1, root tips of 5-d-old PIN2-GFP seedlings and whole roots of 5-d-old BOR1-GFP seedlings were cut for membrane protein extraction (Retzer et al. 2019). Western blotting was done as described before (Wang et al. 2023). The antibodies used include anti-GFP (1:5000 dilution, Utibody, China), anti-H3 (1:5000 dilution, Utibody, China), anti-VDAC1 (1:5000 dilution, Agrisera), anti-COXII (1:5000 dilution, Agrisera), anti-AOX1 (1:5000 dilution, Orizymes, China), anti-ICDH1 (1:5000 dilution, Orizymes, China) and the appropriate IgG-HRP conjugated secondary antibodies (1:5000, ZSGB-Bio, China). The signal was developed using Highly Sensitive ECL Chemiluminescence Substrate (Vazyme, China) and chemiluminescence was detected using a chemiluminescent Western Blot scanner (ChemiScope 6100T, Clinx, China). All experiments were repeated at least three times, and one representative blot was shown.

# Transmission electron microscopy

Five-d-old Col-0 seedlings were treated with liquid ½ MS containing DMSO or AA (10 or 20  $\mu$ M) for 2 h. Root tips (~3 mm) were fixed in 2.5% (v/v) glutaraldehyde overnight, then post-fixed in 1% OsO<sub>4</sub> (w/v) for 2 h. After fixation, samples were rinsed 4 times in 0.1 M phosphate buffer (Na<sub>2</sub>HPO<sub>4</sub>, NaH<sub>2</sub>PO<sub>4</sub>). After dehydration with alcohol and acetone series, samples were embedded in EPON 812 (Ted pella, USA). Ultrathin sections (thickness 70 nm) were cut with a Leica EM UC7 (Leica, Germany), mounted on copper grids and contrasted with TI Blue stainer (Nisshin EM, Japan) and 3% lead citrate solution. The sections were visualized with a Tecnai G2 spirit Biotwin TEM (FEI, USA) at 120 kV accelerating voltage.

# Accession numbers

Accession numbers: PIN1 (AT1G73590), PIN2 (AT5G57090), BOR1 (AT2G47160), AUX1 (AT2G38120), EXPA1 (AT1G69530), EXPA4 (AT2G39700), EXPA6 (AT2G28950), EXPA8 (AT2G40610), EXPA9 (AT5G02260), CEL1 (AT1G70710), KOR1 (AT5G49720), SYP43 (AT3G05710), VHA-a1 (AT2G28520), ARA7 (AT4G19640), RHA1 (AT5G45130), VAMP727 (AT3G54300), VSR4 (AT2G14720), BP80 (AT3G52850), RABG3f (AT3G18820), VAMP711 (AT4G32150), MEMB12 (AT5G50440), SYP32 (AT3G24350).

# Acknowledgments

We thank Drs Xu Wang (Shanghai Jiao Tong University) for ndusf4 seeds, Shengchun Zhang and Chengwei Yang (South China Normal University) for ftsh4 seeds, Lei Li (Nankai University) for lon1-1 seeds, Yiqun Bao (Nanjing Agricultural University) for MEMB12-RFP seeds, Caiji Gao (South China Normal University) for BOR1-GFP, GFP-SYP32, and ST-GFP seeds, Boon Leong Lim (University of Hong Kong) for AT1.03 seeds, Nadine Paris (IPSiM, Univ Montpellier, CNRS, INRAE, Montpellier SupAgro) for Citrine-VSR4 seeds, Ben Scheres (Wageningen University) and Shuzhen Men (Nankai University) for PIN2-GFP seeds, Quan-Sheng Qiu (Lanzhou University) for VHA-a1-GFP, VHA-a1-RFP, and TagRFP-VAMP727 seeds, and Hong Yu (Institute of Genetics and Developmental Biology, Chinese Academy of Sciences) for mito-GFP (3-HA-eGFP-OMP25) seeds. We also thank Ms. Qian Luo from Core Facility and Technical Service Center (Shanghai Jiao Tong University) for help with imaging, and our lab member Yi Yang for discussions. We thank the anonymous reviewers for their insightful suggestions.

## Author contributions

T.W. and Q.G. conceived the project. T.W. performed most of the experiments and analyzed the data. X.L. performed electron microscopy. H.Y. performed some of the experiments. H.Z. and Z.X. contributed essential materials. T.W. and Q.G. drafted the manuscript. H.Z. and Z.X. revised the manuscript. T.W. and Q.G. acquired the funding. All authors approved the manuscript.

# Supplementary data

The following materials are available in the online version of this article.

Supplementary Figure S1. Antimycin A inhibits growth by affecting mitochondrial function.

Supplementary Figure S2. Exogenous ATP can partially rescue Antimycin A-inhibited cell expansion.

Supplementary Figure S3. Antimycin A induces BOR1

Supplementary Figure S4. TGN/EE and MVB/LE are differently affected by AA.

Supplementary Figure S5. Effects of antimycin A on RABG3f and VAMP711.

Supplementary Figure S6. Antimycin A impairs Golgi structure and ERGIC formation.

Supplementary Figure S7. Antimycin A impairs BFA body formation.

**Supplementary Table S1.** Primers used in this study.

Supplementary Video S1. Distribution of the tonoplast marker YFP-VAMP711 after DMSO treatment.

**Supplementary Video S2.** Distribution of VAMP711 after antimycin A treatment.

**Supplementary Video S3.** Distribution of the ERGIC marker MEMB12-RFP after DMSO treatment.

**Supplementary Video S4.** Distribution of MEMB12 after antimycin A treatment.

# **Funding**

This work was supported by grants from the National Natural Science Foundation of China (92354302, 32270726, 91954102, and 31871355), the Natural Science Foundation of Shanghai (23ZR1429400) to QG. TW is supported by Startup Fund for Young Faculty at SJTU (SFYF at SJTU).

Conflict of interest statement. The authors declare no conflict of interest.

# Data availability

The data underlying this article are available in the article and in its online supplementary material.

# References

- Abas L, Benjamins R, Malenica N, Paciorek T, Wiśniewska J, Moulinier-Anzola JC, Sieberer T, Friml J, Luschnig C. Intracellular trafficking and proteolysis of the Arabidopsis auxin-efflux facilitator PIN2 are involved in root gravitropism. *Nat Cell Biol.* 2006:8(3): 249–256. https://doi.org/10.1038/ncb1369
- Aniento F, Sánchez de Medina Hernández V, Dagdas Y, Rojas-Pierce M, Russinova E. Molecular mechanisms of endomembrane trafficking in plants. *Plant Cell*. 2022;34(1):146–173. https://doi.org/10.1093/plcell/koab235
- Berkowitz O, De Clercq I, Van Breusegem F, Whelan J. Interaction between hormonal and mitochondrial signalling during growth, development and in plant defence responses. *Plant Cell Environ*. 2016:39(5):1127–1139. https://doi.org/10.1111/pce.12712
- Cheung AY. FERONIA: a receptor kinase at the core of a global signaling network. *Annu Rev Plant Biol.* 2024:75(1):345–375. https://doi.org/10.1146/annurev-arplant-102820-103424
- Clough SJ, Bent AF. Floral dip: a simplified method for Agrobacterium-mediated transformation of Arabidopsis thaliana. Plant J. 1998:16(6):735–743. https://doi.org/10.1046/j.1365-313x.1998.00343.x
- Cosgrove DJ. Plant expansins: diversity and interactions with plant cell walls. *Curr Opin Plant Biol*. 2015;25:162–172. https://doi.org/10.1016/j.pbi.2015.05.014
- Cui Y, Zhao Q, Gao C, Ding Y, Zeng Y, Ueda T, Nakano A, Jiang L. Activation of the Rab7 GTPase by the MON1-CCZ1 complex is essential for PVC-to-vacuole trafficking and plant growth in Arabidopsis. Plant Cell. 2014:26(5):2080–2097. https://doi.org/10.1105/tpc.114.123141
- Dejonghe W, Kuenen S, Mylle E, Vasileva M, Keech O, Viotti C, Swerts J, Fendrych M, Ortiz-Morea FA, Mishev K, et al. Mitochondrial uncouplers inhibit clathrin-mediated endocytosis largely through cytoplasmic acidification. Nat Commun. 2016;7(1):11710. https://doi.org/10.1038/ncomms11710
- Dejonghe W, Sharma I, Denoo B, De Munck S, Lu Q, Mishev K, Bulut H, Mylle E, De Rycke R, Vasileva M, et al. Disruption of endocytosis through chemical inhibition of clathrin heavy chain function. Nat Chem Biol. 2019:15(6):641–649. https://doi.org/10.1038/s41589-019-0262-1
- Dettmer J, Hong-Hermesdorf A, Stierhof YD, Schumacher K. Vacuolar H+-ATPase activity is required for endocytic and

- secretory trafficking in Arabidopsis. Plant Cell. 2006:18(3): 715–730. https://doi.org/10.1105/tpc.105.037978
- Ebine K, Inoue T, Ito J, Ito E, Uemura T, Goh T, Abe H, Sato K, Nakano A, Ueda T. Plant vacuolar trafficking occurs through distinctly regulated pathways. Curr Biol. 2014:24(12):1375–1382. https://doi.org/10.1016/j.cub.2014.05.004
- Falhof J, Pedersen JT, Fuglsang AT, Palmgren M. Plasma membrane H(+)-ATPase regulation in the center of plant physiology. Mol Plant. 2016:9(3):323–337. https://doi.org/10.1016/j.molp.2015.11.002
- Fougère L, Grison M, Laquel P, Montrazi M, Cordelières F, Fernández-Monreal M, Poujol C, Uemura T, Nakano A, Ito Y, et al. (2023) ER-to-Golgi trafficking via a dynamic intermediate cis-Golgi tubular network in Arabidopsis. bioRxiv https://doi.org/10.1101/2023.10.27.563925
- Garmier M, Carroll AJ, Delannoy E, Vallet C, Day DA, Small ID, Millar AH. Complex I dysfunction redirects cellular and mitochondrial metabolism in Arabidopsis. *Plant Physiol*. 2008:148(3):1324–1341. https://doi.org/10.1104/pp.108.125880
- Gibala M, Kicia M, Sakamoto W, Gola EM, Kubrakiewicz J, Smakowska E, Janska H. The lack of mitochondrial AtFtsH4 protease alters Arabidopsis leaf morphology at the late stage of rosette development under short-day photoperiod. *Plant J.* 2009:59(5):685–699. https://doi.org/10.1111/j.1365-313X.2009.03907.x
- González Solís A, Berryman E, Otegui MS. Plant endosomes as protein sorting hubs. FEBS Lett. 2022:596(17):2288–2304. https://doi.org/10.1002/1873-3468.14425
- Gorman GS, Chinnery PF, DiMauro S, Hirano M, Koga Y, McFarland R, Suomalainen A, Thorburn DR, Zeviani M, Turnbull DM. Mitochondrial diseases. Nat Rev Dis Primers. 2016:2(1):16080. https://doi.org/10.1038/nrdp.2016.80
- Gutierrez R, Lindeboom JJ, Paredez AR, Emons AM, Ehrhardt DW. Arabidopsis cortical microtubules position cellulose synthase delivery to the plasma membrane and interact with cellulose synthase trafficking compartments. Nat Cell Biol. 2009:11(7): 797–806. https://doi.org/10.1038/ncb1886
- Hao L, Liu J, Zhong S, Gu H, Qu LJ. AtVPS41-mediated endocytic pathway is essential for pollen tube-stigma interaction in Arabidopsis. Proc Natl Acad Sci U S A. 2016:113(22):6307–6312. https://doi.org/10.1073/pnas.1602757113
- Haruta M, Sabat G, Stecker K, Minkoff BB, Sussman MR. A peptide hormone and its receptor protein kinase regulate plant cell expansion. Science. 2014:343(6169):408–411. https://doi.org/10.1126/science. 1244454
- Hawkins TJ, Kopischke M, Duckney PJ, Rybak K, Mentlak DA, Kroon JTM, Bui MT, Richardson AC, Casey M, Alexander A, et al. NET4 and RabG3 link actin to the tonoplast and facilitate cytoskeletal remodelling during stomatal immunity. Nat Commun. 2023:14(1):5848. https://doi.org/10.1038/s41467-023-41337-z
- Hedrich R, Sauer N, Neuhaus HE. Sugar transport across the plant vacuolar membrane: nature and regulation of carrier proteins. *Curr Opin Plant Biol.* 2015:25:63–70. https://doi.org/10.1016/j.pbi. 2015.04.008
- Imamura H, Nhat KP, Togawa H, Saito K, Iino R, Kato-Yamada Y, Nagai T, Noji H. Visualization of ATP levels inside single living cells with fluorescence resonance energy transfer-based genetically encoded indicators. Proc Natl Acad Sci U S A. 2009:106(37): 15651–15656. https://doi.org/10.1073/pnas.0904764106
- Ivanova A, Law SR, Narsai R, Duncan O, Lee JH, Zhang B, Van Aken O, Radomiljac JD, van der Merwe M, Yi K, et al. A functional antagonistic relationship between auxin and mitochondrial retrograde signaling regulates alternative oxidase1a expression in Arabidopsis. Plant Physiol. 2014:165(3):1233–1254. https://doi.org/10.1104/pp. 114.237495

- Jamieson JD, Palade GE. Intracellular transport of secretory proteins in the pancreatic exocrine cell. IV. Metabolic requirements. J Cell Biol. 1968:39(3):589-603. https://doi.org/10.1083/jcb.39.3.589
- Jásik J, Bokor B, Stuchlík S, Mičieta K, Turňa J, Schmelzer E. Effects of auxins on PIN-FORMED2 (PIN2) dynamics are not mediated by inhibiting PIN2 endocytosis. Plant Physiol. 2016:172(2):1019-1031. https://doi.org/10.1104/pp.16.00563
- Kerchev PI, De Clercq I, Denecker J, Mühlenbock P, Kumpf R, Nguyen L, Audenaert D, Dejonghe W, Van Breusegem F. Mitochondrial perturbation negatively affects auxin signaling. Mol Plant. 2014:7(7):1138-1150. https://doi.org/10.1093/mp/ssu071
- Kim DH, Eu YJ, Yoo CM, Kim YW, Pih KT, Jin JB, Kim SJ, Stenmark H, Hwang I. Trafficking of phosphatidylinositol 3-phosphate from the trans-Golgi network to the lumen of the central vacuole in plant cells. Plant Cell. 2001:13(2):287-301. https://doi.org/10.1105/tpc.13.2.287
- Laxmi A, Pan J, Morsy M, Chen R. Light plays an essential role in intracellular distribution of auxin efflux carrier PIN2 in Arabidopsis thaliana. PLoS One. 2008:3(1):e1510. https://doi.org/10.1371/ journal.pone.0001510
- Li Y, Zeng H, Xu F, Yan F, Xu W. H(+)-ATPases in plant growth and stress responses. Annu Rev Plant Biol. 2022:73(1):495-521. https:// doi.org/10.1146/annurev-arplant-102820-114551
- Luo Y, Scholl S, Doering A, Zhang Y, Irani NG, Rubbo SD, Neumetzler L, Krishnamoorthy P, Van Houtte I, Mylle E, et al. V-ATPase activity in the TGN/EE is required for exocytosis and recycling in Arabidopsis. Nat Plants. 2015:1(7):15094. https://doi.org/10.1038/ nplants.2015.94
- Ma J, Liang Z, Zhao J, Wang P, Ma W, Mai KK, Fernandez Andrade JA, Zeng Y, Grujic N, Jiang L, et al. Friendly mediates membrane depolarization-induced mitophagy in Arabidopsis. Curr Biol. 2021:31(9):1931-1944.e4. https://doi.org/10.1016/j.cub.2021.02.034
- Marchant A, Kargul J, May ST, Muller P, Delbarre A, Perrot-Rechenmann C, Bennett MJ. AUX1 regulates root gravitropism in Arabidopsis by facilitating auxin uptake within root apical tissues. EMBO J. 1999:18(8):2066-2073. https://doi.org/10.1093/ emboj/18.8.2066
- Martin W, Müller M. The hydrogen hypothesis for the first eukaryote. Nature. 1998:392(6671):37-41. https://doi.org/10.1038/32096
- Martinoia E. Vacuolar transporters—companions on a longtime journey. Plant Physiol. 2018:176(2):1384-1407. https://doi.org/10.1104/ pp.17.01481
- Meyer EH, Tomaz T, Carroll AJ, Estavillo G, Delannoy E, Tanz SK, Small ID, Pogson BJ, Millar AH. Remodeled respiration in ndufs4 with low phosphorylation efficiency suppresses Arabidopsis germination and growth and alters control of metabolism at night. Plant Physiol. 2009:151(2):603-619. https://doi.org/10.1104/pp.109.141770
- Millar AH, Whelan J, Soole KL, Day DA. Organization and regulation of mitochondrial respiration in plants. Annu Rev Plant Biol. 2011:62(1): 79–104. https://doi.org/10.1146/annurev-arplant-042110-103857
- Minamino N, Ueda T. RAB GTPases and their effectors in plant endosomal transport. Curr Opin Plant Biol. 2019:52:61-68. https://doi. org/10.1016/j.pbi.2019.07.007
- Møller IM, Rasmusson AG, Van Aken O. Plant mitochondria—past, present and future. Plant J. 2021:108(4):912-959. https://doi.org/ 10.1111/tpj.15495
- Mossessova E, Corpina RA, Goldberg J. Crystal structure of ARF1\*Sec7 complexed with Brefeldin A and its implications for the guanine nucleotide exchange mechanism. Mol Cell. 2003:12(6):1403-1411. https://doi.org/10.1016/S1097-2765(03)00475-1
- Neuhaus HE, Trentmann O. Regulation of transport processes across the tonoplast. Front Plant Sci. 2014:5:460. https://doi.org/10.3389/ fpls.2014.00460

- Nunnari J., Suomalainen A. Mitochondria: in sickness and in health. Cell. 2012:148(6):1145-1159. https://doi.org/10.1016/j.cell.2012.02.035
- Ohbayashi I, Huang S, Fukaki H, Song X, Sun S, Morita MT, Tasaka M, Millar AH, Furutani M. Mitochondrial pyruvate dehydrogenase contributes to auxin-regulated organ development. Plant Physiol. 2019:180(2):896-909. https://doi.org/10.1104/pp.18.01460
- Pfanner N, Warscheid B, Wiedemann N. Mitochondrial proteins: from biogenesis to functional networks. Nat Rev Mol Cell Biol. 2019:20(5):267-284. https://doi.org/10.1038/s41580-018-0092-0
- Rasmusson AG, Svensson AS, Knoop V, Grohmann L, Brennicke A. Homologues of yeast and bacterial rotenone-insensitive NADH dehydrogenases in higher eukaryotes: two enzymes are present in potato mitochondria. Plant J. 1999:20(1):79-87. https://doi.org/ 10.1046/j.1365-313X.1999.00576.x
- Retzer K, Akhmanova M, Konstantinova N, Malínská K, Leitner J, Petrášek J, Luschnig C. Brassinosteroid signaling delimits root gravitropism via sorting of the Arabidopsis PIN2 auxin transporter. Nat Commun. 2019:10(1):5516. https://doi.org/10.1038/s41467-019-13543-1
- Rigas S, Daras G, Laxa M, Marathias N, Fasseas C, Sweetlove LJ, Hatzopoulos P. Role of Lon1 protease in post-germinative growth and maintenance of mitochondrial function in Arabidopsis thaliana. New Phytol. 2009:181(3):588-600. https://doi.org/10.1111/j. 1469-8137.2008.02701.x
- Rodriguez-Furlan C, Domozych D, Qian W, Enquist PA, Li X, Zhang C, Schenk R, Winbigler HS, Jackson W, Raikhel NV, et al. Interaction between VPS35 and RABG3f is necessary as a checkpoint to control fusion of late compartments with the vacuole. Proc Natl Acad Sci U S A. 2019:116(42):21291–21301. https://doi.org/10.1073/pnas. 1905321116
- Roger AJ, Muñoz-Gómez SA, Kamikawa R. The origin and diversification of mitochondria. Curr Biol. 2017:27(21):R1177-R1192. https:// doi.org/10.1016/j.cub.2017.09.015
- Rui Q, Tan X, Liu F, Li Y, Liu X, Li B, Wang J, Yang H, Qiao L, Li T, et al. Syntaxin of plants31 (SYP31) and SYP32 is essential for Golgi morphology maintenance and pollen development. Plant Physiol. 2021:186(1):330-343. https://doi.org/10.1093/plphys/kiab049
- Saint-Jore CM, Evins J, Batoko H, Brandizzi F, Moore I, Hawes C. Redistribution of membrane proteins between the Golgi apparatus and endoplasmic reticulum in plants is reversible and not dependent on cytoskeletal networks. Plant J. 2002:29(5):661–678. https://doi.org/10.1046/j.0960-7412.2002.01252.x
- Schaller GE, Bishopp A, Kieber JJ. The yin-yang of hormones: cytokinin and auxin interactions in plant development. Plant Cell. 2015:27(1):44-63. https://doi.org/10.1105/tpc.114.133595
- Schertl P, Braun HP. Respiratory electron transfer pathways in plant mitochondria. Front Plant Sci. 2014:5:163. https://doi.org/10.3389/ fpls.2014.00163
- Schwarzländer M, Fricker MD, Sweetlove LJ. Monitoring the in vivo redox state of plant mitochondria: effect of respiratory inhibitors, abiotic stress and assessment of recovery from oxidative challenge. Biochim Biophys Acta. 2009:1787(5):468-475. https://doi. org/10.1016/j.bbabio.2009.01.020
- Smith AM. Prospects for increasing starch and sucrose yields for bioethanol production. Plant J. 2008:54(4):546–558. https://doi.org/10. 1111/j.1365-313X.2008.03468.x
- Spang A, Saw JH, Jørgensen SL, Zaremba-Niedzwiedzka K, Martijn J, Lind AE, van Eijk R, Schleper C, Guy L, Ettema TJG. Complex archaea that bridge the gap between prokaryotes and eukaryotes. Nature. 2015:521(7551):173-179. https://doi.org/10.1038/nature14447
- Suomalainen A, Nunnari J. Mitochondria at the crossroads of health and disease. Cell. 2024:187(11):2601-2627. https://doi.org/10.1016/ j.cell.2024.04.037

- Szymanski D, Staiger CJ. The actin cytoskeleton: functional arrays for cytoplasmic organization and cell shape control. *Plant Physiol.* 2018:176(1):106–118. https://doi.org/10.1104/pp.17.01519
- Takano J, Noguchi K, Yasumori M, Kobayashi M, Gajdos Z, Miwa K, Hayashi H, Yoneyama T, Fujiwara T. Arabidopsis boron transporter for xylem loading. *Nature*. 2002:420(6913):337–340. https://doi.org/10.1038/nature01139
- Takano J, Tanaka M, Toyoda A, Miwa K, Kasai K, Fuji K, Onouchi H, Naito S, Fujiwara T. Polar localization and degradation of Arabidopsis boron transporters through distinct trafficking pathways. Proc Natl Acad Sci U S A. 2010:107(11):5220–5225. https://doi.org/10.1073/pnas.0910744107
- Takemoto K, Ebine K, Askani JC, Krüger F, Gonzalez ZA, Ito E, Goh T, Schumacher K, Nakano A, Ueda T. Distinct sets of tethering complexes, SNARE complexes, and Rab GTPases mediate membrane fusion at the vacuole in Arabidopsis. Proc Natl Acad Sci U S A. 2018:115(10):E2457–eE2466. https://doi.org/10.1073/pnas.1717839115
- Tivendale ND, Belt K, Berkowitz O, Whelan J, Millar AH, Huang S. Knockdown of succinate dehydrogenase assembly factor 2 induces reactive oxygen species-mediated auxin hypersensitivity causing pH-dependent root elongation. *Plant Cell Physiol*. 2021;62(7):1185–1198. https://doi.org/10.1093/pcp/pcab061
- Tivendale ND, Millar AH. How is auxin linked with cellular energy pathways to promote growth? *New Phytol.* 2022:233(6):2397–2404. https://doi.org/10.1111/nph.17946
- Tjaden J, Möhlmann T, Kampfenkel K, Henrichs G, Neuhaus HE. Altered plastidic ATP/ADP-transporter activity influences potato (L.) tuber morphology, yield and composition of tuber starch. Plant J. 1998:16(5):531–540. https://doi.org/10.1046/j.1365-313x. 1998.00317.x
- Uemura T, Kim H, Saito C, Ebine K, Ueda T, Schulze-Lefert P, Nakano A. Qa-SNAREs localized to the trans-Golgi network regulate multiple transport pathways and extracellular disease resistance in plants. *Proc Natl Acad Sci U S A*. 2012:109(5):1784–1789. https://doi.org/10.1073/pnas.1115146109
- Uemura T, Ueda T, Ohniwa RL, Nakano A, Takeyasu K, Sato MH.
  Systematic analysis of SNARE molecules in Arabidopsis:

- dissection of the post-Golgi network in plant cells. *Cell Struct Funct*. 2004:29(2):49–65. https://doi.org/10.1247/csf.29.49
- Vera-Maldonado P, Aquea F, Reyes-Díaz M, Cárcamo-Fincheira P, Soto-Cerda B, Nunes-Nesi A, Inostroza-Blancheteau C. Role of boron and its interaction with other elements in plants. Front Plant Sci. 2024:15:1332459. https://doi.org/10.3389/fpls.2024.1332459
- Wang T, Li X, Liu N, Yang Y, Gong Q. TurboID-based proximity labelling reveals a connection between VPS34 and cellular homeostasis. J Plant Physiol. 2023:289:154100. https://doi.org/10.1016/j.jplph. 2023.154100
- Wong YC, Ysselstein D, Krainc D. Mitochondria-lysosome contacts regulate mitochondrial fission via RAB7 GTP hydrolysis. *Nature*. 2018:554(7692):382–386. https://doi.org/10.1038/nature25486
- Yang Y, Hammes UZ, Taylor CG, Schachtman DP, Nielsen E. High-affinity auxin transport by the AUX1 influx carrier protein. Curr Biol. 2006:16(11):1123–1127. https://doi.org/10.1016/j.cub. 2006.04.029
- Zeng Y, Liang Z, Liu Z, Li B, Cui Y, Gao C, Shen J, Wang X, Zhao Q, Zhuang X, et al. Recent advances in plant endomembrane research and new microscopical techniques. New Phytol. 2023:240(1):41–60. https://doi.org/10.1111/nph.19134
- Zhang C, Hicks GR, Raikhel NV. Plant vacuole morphology and vacuolar trafficking. Front Plant Sci. 2014a:5:476. https://doi.org/10.3389/fpls.2014.00476
- Zhang S, Wu J, Yuan D, Zhang D, Huang Z, Xiao L, Yang C. Perturbation of auxin homeostasis caused by mitochondrial FtSH4 gene-mediated peroxidase accumulation regulates arabidopsis architecture. *Mol Plant.* 2014b:7(5):856–873. https://doi.org/10.1093/mp/ssu006
- Zheng J, Han SW, Rodriguez-Welsh MF, Rojas-Pierce M. Homotypic vacuole fusion requires VTI11 and is regulated by phosphoinositides. Mol Plant. 2014:7(6):1026–1040. https://doi.org/10.1093/mp/ssu019
- Zheng W, Chai P, Zhu J, Zhang K. High-resolution in situ structures of mammalian respiratory supercomplexes. *Nature*. 2024:631(8019): 232–239. https://doi.org/10.1038/s41586-024-07488-9
- Zhuang X, Li R, Jiang L. A century journey of organelles research in the plant endomembrane system. Plant Cell. 2024:36(5): 1312–1333. https://doi.org/10.1093/plcell/koae004